

A model of light pseudoscalar dark matter

Shreyashi Chakdar,^{1,*} Dilip Kumar Ghosh,^{2,†} P. Q.

Hung,^{3,‡} Najimuddin Khan,^{2,§} and Dibyendu Nanda^{2,¶}

¹*Department of Physics, College of the Holy Cross, Worcester, MA 01610, USA*

²*School of Physical Sciences, Indian Association for the Cultivation of Science,
2A & 2B Raja S.C. Mullick Road, Kolkata 700032, India*

³*Department of Physics, University of Virginia, Charlottesville, VA 22904-4714, USA*

Abstract

The EW- ν_R model was constructed in order to provide a seesaw scenario operating at the Electroweak scale $\Lambda_{EW} \sim 246$ GeV, keeping the same SM gauge structure. In this model, right-handed neutrinos are non-sterile and have masses of the order of Λ_{EW} . They can be searched for at the LHC along with heavy mirror quarks and leptons, the lightest of which have large decay lengths. The seesaw mechanism requires the existence of a complex scalar which is singlet under the SM gauge group. The imaginary part of this complex scalar denoted by A_s^0 is proposed to be the sub-MeV dark matter candidate in this manuscript. We find that the sub-MeV scalar can serve as a viable non-thermal feebly interacting massive particle (FIMP)-DM candidate. This A_s^0 can be a naturally light sub-MeV DM candidate due to its nature as a pseudo-Nambu-Goldstone (PNG) boson in the model. We show that the well-studied freeze out mechanism falls short in this particular framework producing DM overabundance. We identify that the freeze in mechanism produce the correct order of relic density for the sub-MeV DM candidate satisfying all applicable constraints. We then discuss the DM parameter space allowed by the current bounds from the direct and indirect searches for this sub-MeV DM. This model has a very rich scalar sector, consistent with various experimental constraints, predicts a ~ 125 GeV scalar with the SM Higgs characteristics satisfying the current LHC Higgs boson data.

* Email Address: schakdar@holycross.edu

† Email Address: tpdkg@iacs.res.in

‡ Email Address: pqh@virginia.edu

§ Email Address: psnk2235@iacs.res.in

¶ Email Address: psdn2502@iacs.res.in

I. INTRODUCTION AND FRAMEWORK

The various astronomical and cosmological evidences, like rotation curves of spatial galaxies [1, 2], gravitational lensing [3], the bullet cluster [4] etc., vindicate the existence of dark matter (DM). The Planck Collaboration [5] using the precise map of the cosmic microwave background (CMB) indicates that DM contributes almost 26% to the mass/energy budget of the universe. These observations can most plausibly be explained by postulating the existence of particles which interact either very weakly with ordinary particles or only through gravity. However, the nature of dark matter in the form of particles is still elusive. The failure of the standard model (SM) of particle physics to account for a viable DM candidate, opens up the pathway of various scenarios beyond the standard model (BSM) to resolve the DM puzzle.

The most studied example of DM in any BSM scenario is the so-called weakly interacting massive particle (WIMP) with mass close to the Electroweak scale and weak couplings with the SM particles. In this scenario, once WIMPs are thermally produced at the very early universe, depending upon its mass and interaction strength remain in thermal equilibrium with the SM bath up to a certain temperature. Eventually they decouple from the thermal bath at some temperature T_f , which is commonly called the *Freeze-out* temperature, where the DM interaction rate dropped below the expansion rate of the Universe, governed by the Hubble parameter H . At that point, the DM freezes-out from the SM thermal bath providing the observed DM relic density, which is only affected by the expansion of the universe. It is very interesting to note that in the WIMP scenario, the theoretical prediction of the DM thermal relic density coincides very well with the observed DM relic abundance ($\Omega h^2 \sim 0.12$ [5]), popularly known as the *WIMP-miracle*. In spite of this WIMP miracle, however, various null results from the WIMP searches at LHC [6–10], at the spin independent and dependent WIMP-nucleon scattering experiments at LUX [11], PANDAX-II [12], XENON-1T [13], PICO [14] etc. and from the indirect detection coming from FERMI-LAT [15] MAGIC [16] and PLANCK [5] experiments have excluded a significant part in the parameter space of the WIMP-nucleon scattering cross-section vs WIMP mass plane. As the various WIMP searches continue to provide null results, one either plans completely new search techniques for WIMP detection other than the aforementioned scattering experiments [17] or moves away from the WIMP paradigm completely towards an alternative scenario, where the DM particles have very

feeble interactions with SM and never enters the thermal bath. However in this case, DM obtain their relic abundance very slowly through the decay and/or the annihilation of the bath particles, known as the *Freeze-in* process, providing a completely different solution to the DM conundrum [18, 19]. For such cases, the production of DM from the decays will contribute dominantly if the same couplings are involved in both decay and annihilation. Due to such feeble interactions, it is extremely challenging to detect the DM in the present direct search experiments. However, many new experiment techniques with low-threshold direct detection[20–25] have been proposed that have the capability to probe FIMPs in the near future. Particularly, for a MeV scale feebly interacting massive particle (FIMP), having interaction with electron could be tested by next generation experiments[20, 21, 26] and one can constrain the typical DM-electron cross sections. In case of light DM, their number density have to be very large to satisfy the observed relic abundance that can enhance their detection rate.

In this paper, we will present a framework for a sub-MeV DM arising naturally from the theoretical construction of our model. However, our detailed knowledge of nucleosynthesis puts a strong constraint on the thermal production of such sub-MeV DM. In particular, this kind of DM could be overabundant if produced by a thermal freeze-out mechanism and motivated by this fact, here we have studied the non-thermal production of such MeV-scale DM. In building such a model for the sub-MeV DM, it is legitimate to ask how natural is it to have such a light (sub-MeV) particle and how it could satisfy the aforementioned constraints. This work is based on a model (the EW- ν_R model) proposed by one of us [27] of non-sterile right-handed neutrinos with Majorana masses being proportional to the Electroweak scale $\Lambda_{EW} = 246$ GeV and, as a result, can be produced and searched for at the Large Hadron Collider (LHC). To see how the EW- ν_R model generates a light DM particle, a brief summary of the seesaw mechanism of the model is in order. The model contains mirror fermions and, for the purpose of this introduction, it is sufficient to discuss one generation of SM leptons: $\psi_L = (\nu_\ell, \ell)^T_L$; ℓ_R , and mirror leptons: $\psi_R^M = (\nu_\ell^M, \ell^M)^T_R$; ℓ_L^M . The Majorana mass for right-handed neutrinos is obtained by coupling ℓ_R^M to a complex Higgs triplet $\tilde{\chi}$ as $y_M \psi_R^{M,T} \sigma_2(\tau_2 \tilde{\chi}) \psi_R^M$. With $\langle \tilde{\chi} \rangle = v_M$, one obtains $M_R = \frac{y_M v_M}{\sqrt{2}}$. Right-handed neutrinos in this model, being non-sterile, have to be heavier than $M_Z/2$ constrained by the Z -width data, implying that $v_M \propto \Lambda_{EW}$ severely affects the custodial symmetry which ensures that $M_W = M_Z \cos \theta_W$ at tree-level. Custodial symmetry is restored by the introduction of real triplet ξ having the same

VEV as $\tilde{\chi}$. (It turns out that this real triplet also provides a solution for a topologically stable, finite energy electroweak monopole [28, 29].) The Dirac mass term in this seesaw mechanism comes from the coupling of a SM left-handed lepton doublet, a mirror right-handed lepton doublet with a *complex singlet scalar* Φ_s : $y_{s\ell} \bar{\ell}_L \Phi_s \ell_R^M + \text{h.c.}$, giving $m_D = y_{s\ell} v_s$ when $\langle \Phi_s \rangle = v_s$. As we show below, the imaginary part of this complex singlet Φ_s which is a pseudo-Nambu-Goldstone (PNG) boson, A_s^0 , can be used as a light DM candidate, for the simple reason that A_s^0 would be massless when a global symmetry present in the EW- ν_R model is spontaneously broken. A_s^0 acquires a mass when there is an explicit breaking term in the scalar potential. As one has encountered similar situations in various places such as chiral symmetry breaking, the explicit breaking term is characterized by some mass scale which is usually assumed to be much smaller than the scale of spontaneous symmetry breaking (SSB): the global symmetry is an approximate symmetry. For example, hadronic $SU(2)_L \times SU(2)_R$ is an approximate symmetry with the SSB scale $\Lambda_{QCD} \approx 300\text{MeV}$ and the scales of explicit breaking are the up and down quarks masses, 2.3 MeV and 4.8 MeV. As we shall see below, the SSB scale of the aforementioned global symmetry is of the order of the Electroweak scale and the explicit breaking scale is the mass of A_s^0 which will be assumed to be in the sub-MeV region. This PNG boson A_s^0 will be an ideal sub-MeV DM candidate.

It will be shown that the production of A_s^0 through a Freeze-out mechanism is not preferred since it will be overabundant. It will further be shown that the Freeze-in mechanism is the most attractive alternate possibilities in this scenario. As A_s^0 interacts very feebly with other particles (FIMP), it can be non-thermally produced through a Freeze-in mechanism, yielding the correct relic density and satisfying constraints from direct and indirect searches. The model contains a large parameter space exhibiting the aforementioned behavior of our DM candidate. From a particle physics point of view, this DM scenario has a very interesting implication concerning the seesaw mechanism of the EW- ν_R model: the symmetry breaking scales proportional to the Dirac and Majorana masses as described in the previous paragraphs are found to be comparable in sizes, avoiding the kind of hierarchy found in a generic seesaw mechanism.

The organization of the paper is as follows. In Section II, we present the framework for the rich scalar sector for the EW- ν_R model. Section III contains the influence of various theoretical and experimental constraints on the model parameters. In Section IV we present our selection of benchmark points and discuss the various LHC bounds examining the stability of this kind of

light dark matter candidate. Section V discusses how $A_s^0 (\equiv \text{Im}(\Phi_s))$, a pseudo-Nambu Goldstone boson can successfully play the role of a potential sub-MeV dark matter in this framework and section VI includes how the FIMP dark matter candidate A_s^0 produces the correct relic density. Section VII discusses the constraints pertaining to the indirect and direct searches. The summary and implications are presented in Section VIII. Finally, the Appendix is devoted to a collection of detailed results and formulae pertaining to the analysis of the complete scalar sector and the previous sections.

II. EXTENDED SCALAR SECTOR OF THE MODEL

The main idea of the EW- ν_R model [30] containing mirror fermions including Majorana masses for right-handed neutrinos proportional to the Electroweak scale with an extended scalar sector is very appealing. Unlike the Standard Model, the framework is not only left-right symmetric, but each left handed fermion multiplet is accompanied by new right handed fermion multiplet of opposite chirality. The framework contains a rich scalar sector incorporating four doublets (two belonging to the Two Higgs doublet model-THDM like Φ_1, Φ_2 , two for mirror sector Φ_{1M}, Φ_{2M}), two triplets $\tilde{\chi}, \xi$ and one complex singlet Φ_s it represented by

$$\Phi_1 = \begin{pmatrix} \phi_1^{0,*} & \phi_1^+ \\ \phi_1^- & \phi_1^0 \end{pmatrix}, \quad \Phi_{1M} = \begin{pmatrix} \phi_{1M}^{0,*} & \phi_{1M}^+ \\ \phi_{1M}^- & \phi_{1M}^0 \end{pmatrix}, \quad \Phi_2 = \begin{pmatrix} \phi_2^{0,*} & \phi_2^+ \\ \phi_2^- & \phi_2^0 \end{pmatrix}, \quad \Phi_{2M} = \begin{pmatrix} \phi_{2M}^{0,*} & \phi_{2M}^+ \\ \phi_{2M}^- & \phi_{2M}^0 \end{pmatrix},$$

$$\tilde{\chi} = \begin{pmatrix} \chi^+/\sqrt{2} & \chi^{++} \\ \chi^0 & -\chi^+/\sqrt{2} \end{pmatrix}, \quad \xi = (\xi^+, \xi^0, \xi^-), \quad \Phi_s$$
(2.1)

The Higgs potential consisting of these scalars has a global $SU(2)_L \times SU(2)_R$ symmetry, under which the triplet and doublet scalars transform as (3,3) and (2,2)¹. The Electroweak symmetry is spontaneously broken by the VEVs of the neutral component of the doublet and triplet scalars. We denote VEVs of the scalar fields $\Phi_1, \Phi_2, \Phi_{1M}, \Phi_{2M}, \chi$ and Φ_s as $v_1, v_2, v_{1M}, v_{2M}, v_M$ and v_s respectively, where, χ field is the combination of two triplet scalars $\tilde{\chi}$ and ξ (see eqns.A1-A5). The standard model vacuum expectation value is given by, $v_{\text{SM}} \equiv \sqrt{v_1^2 + v_2^2 + v_{1M}^2 + v_{2M}^2 + 8v_M^2} \approx 246$ GeV. After the spontaneous Electroweak symmetry breaking, the VEVs are aligned in such a

¹ The transformation $(SU(2)_L$ triplet, $SU(2)_R$ triplet) \equiv (3,3) and the doublet transformation is denoted by (2,2).

manner that there still remains an unbroken $SU(2)_D$ custodial symmetry, ie. $SU(2)_L \times SU(2)_R \rightarrow SU(2)_D$ and we get six $SU(2)_D$ singlet CP-even Higgs like scalars ($H_1^0, H_2^0, H_{1M}^0, H_{2M}^0, H_s^0, H_1^{0'}$), forming a 6×6 matrix $\mathcal{M}_{\mathcal{H}}^2$. We obtain the physical eigenstates \tilde{H}'''' , \tilde{H}''' , \tilde{H}'' , \tilde{H}' , \tilde{H} , \tilde{H}_s , in descending order of mass ($M_{\tilde{H}''''} > M_{\tilde{H}''' > M_{\tilde{H}''} > M_{\tilde{H}'} > M_{\tilde{H}} > M_{\tilde{H}_s}$) after diagonalizing $\mathcal{M}_{\mathcal{H}}^2$ by an orthogonal matrix O_H . Among these new physical scalars, \tilde{H} behaves as the SM like 125 GeV Higgs observed at the LHC. This SM like Higgs boson state is expressed as a superposition of 6 weak eigenstates as: $\tilde{H} = O_H^{51} H_1^0 + O_H^{52} H_2^0 + O_H^{53} H_{1M}^0 + O_H^{54} H_{2M}^0 + O_H^{55} H_s^0 + O_H^{56} H_1^{0'}$. The mixing angles O_H^{51} and O_H^{52} control the coupling of \tilde{H} with various standard model particles through the SM like $SU(2)_L$ doublet scalars H_1^0 and H_2^0 respectively. The detailed analysis on the extended scalar sector of this present framework have been discussed in the Appendix A.

III. THEORETICAL AND EXPERIMENTAL CONSTRAINTS ON THE MODEL

The particle spectrum of this model include additional charged fermions and scalars that interact with the standard model sector leading to non-trivial theoretical implications as well experimental observations. In this section we look at various theoretical and experimental constraints on the model parameters:

- **Perturbativity :** The values of various quartic couplings of the Higgs potential are chosen to be perturbative : $|\lambda_i| < 4\pi$, where λ_i s are defined in the Appendix A. The Yukawa couplings are taken to be $< \sqrt{4\pi}$.
- **Constraints from electroweak precision observables :** The additional mirror fermions and heavy $SU(2)$ doublet and triplet scalars contribute to the electroweak precision observable, namely the oblique S,T, & U parameters [31]. It should be noted that constraints coming from these parameters have been worked out in Ref. [32] for an earlier version of the model where only two Higgs doublets were incorporated (in addition to the two triplets and the singlet). As shown in Ref. [32], the main contributions that can offset the positive contributions from the new mirror fermions to the S and T parameters come from the triplets which are negative. Additional Higgs doublets will not alter this picture and we preserve the characteristic of the earlier version of the model. Nevertheless, in our numerical analysis, we

have applied the constraints on the mass difference between the doubly, singly charged and neutral scalars and between the mirror *up*–*down* fermions of the $SU(2)$ fermion doublets, $\Delta M_{5,ij} \equiv |M_i - M_j|$ (where $i \neq j$, $i, j = H_5^{\pm\pm}, H_5^\pm$ and H_5^0), $\Delta M_3 \equiv |M_{H_3^\pm} - M_{H_3^0}|$ and $\Delta M_f \equiv |M_{f_{MF}^{u,\nu_R}} - M_{f_{MF}^{d,l}}|$ to be less than ~ 50 GeV coming from the T-parameter constraint with the assumption of a light SM like Higgs boson with 125 GeV mass and 173.1 GeV top quark mass. For our choice of benchmark points all the aforementioned scalar and mirror up-down masses are almost unchanged, thus automatically satisfying the T-parameter constraints [32].

- **Constraints from Lepton Flavor Violating processes :** The presence of mirror leptons would lead to additional contribution to $\mu \rightarrow e\gamma$ at the one loop level and $\mu \rightarrow 3e$ as well as $\tau \rightarrow 3\ell$ processes [33] at the tree level due to the charged lepton mixing through the Yukawa interaction $y_{s\ell}\bar{\psi}_L\psi_R^M\Phi_s$. Among all the aforementioned LFV processes, the most stringent limit comes from $\mu \rightarrow e\gamma$ process. From the MEG experiment at PSI, we get the most stringent limit $\text{BR}(\mu^+ \rightarrow e^+\gamma) < 4.2 \times 10^{-13}$ at 90% C.L. [34, 35]. On the other hand for μ to e conversion in the nuclei, the current experimental upper limits on branching ratios are provided by the SINDRUM II experiment for gold and titanium targets, $\text{BR}(\mu^- + \text{Au} \rightarrow e^- + \text{Au}) < 7 \times 10^{-13}$ and $\text{BR}(\mu^- + \text{Ti} \rightarrow e^- + \text{Ti}) < 4.3 \times 10^{-12}$ respectively at 90% C.L. [35, 36]. The current experimental upper limit on $\text{Br}(\mu \rightarrow e\gamma)$ sets a stringent limit on $y_{s\ell} \leq 10^{-4}$ for the mirror lepton mass $M_{f_{MF}} \sim 100 - 800$ GeV [37–39]. It is also important to note that the most stringent constraint are placed on the additional couplings $y_s \sim y_{sq} \sim y_{su} \sim y_{sd}$ from the solution of the strong CP problem. The previous studies by one us has pointed out such limit as $y_s < 0.1y_{s\ell}$ [40, 41].
- **The Higgs signal strength :** It is to be noted that the experimentally measured properties of the 125-GeV scalar particle discovered at the LHC so far tend to favor the characteristics of SM Higgs boson. Hence, in every beyond standard model scenario, it is necessary to have at least one of the scalars with mass ~ 125 GeV satisfying the experimental Higgs signal strengths data. In the present scenario, we have a rich scalar sector and mirror fermions. After the spontaneous Electroweak symmetry breaking, various scalars and fermions would mix among themselves, and thus causing deviations in the coupling for the SM like Higgs

boson with the SM fermions and gauge bosons at tree level. These modified couplings and new scalars and fermions would affect the SM like Higgs production as well as decay modes into various final states. This deviation is parametrized in terms of various Higgs signal strengths, defined as $\mu_X = \frac{\sigma(pp \rightarrow \tilde{H})_{\text{BSM}}}{\sigma(pp \rightarrow h)_{\text{SM}}} \frac{BR(\tilde{H} \rightarrow X)_{\text{BSM}}}{BR(h \rightarrow X)_{\text{SM}}}$, where, $X = \gamma\gamma, W^+W^-, ZZ, b\bar{b}$ and $\tau^+\tau^-$. In Table III, we show the CMS best fit $\mu_{\text{Best-Fit}}$ for the combined measurements of the Higgs signal strengths at 13 TeV run of the LHC with 35.9 fb^{-1} data [42]. However, any deviation in the aforementioned Higgs signal strengths would be highly dependent on the choice of model parameters as shown in Table I. We will discuss these benchmark points in the next section.

	Benchmark Points															Masses of the scalar fields (GeV)								
	VEV of the scalar fields (GeV)					Scalar quartic couplings λ 's																		
	v_1	v_2	v_{1M}	v_{2M}	v_M	v_s	λ_{1a}	λ_{1b}	λ_{2a}	λ_{2b}	λ_3	λ_4	λ_5	λ_8	λ_s	$M_{\tilde{H}'''}$	$M_{\tilde{H}''}$	$M_{\tilde{H}''}$	$M_{\tilde{H}'}$	$M_{\tilde{H}}$	$M_{\tilde{H}_s}$	m_5	m_{3,H^\pm, H_3^0}	$m_{3,\text{All others}}$
BP-1 52.04% Φ_1 , 47.95% Φ_2	140	145	43.5	43.5	45	10^4	0.09	0.1	9.0	9.0	9.0	2.9	9.0	9.0	10^{-14}	1126.12	607.15	369.85	352.90	124.16	0.0028	1279.4	738.66	972.59
BP-2 51.52% Φ_1 , 48.47% Φ_2	138	142	51.07	51.07	45	10^4	0.1	0.1	9.0	9.0	9.0	2.9	9.0	9.0	10^{-14}	1130.13	610.94	433.36	402.58	125.18	0.0028	1279.4	738.66	972.34
BP-3 51.52% Φ_1 , 48.47% Φ_2	152	145	42.99	42.99	40	10^4	0.001	0.1	9.0	9.0	9.0	0.5	9.0	9.0	10^{-14}	622.02	454.13	364.76	337.63	125.82	0.0028	1279.4	738.66	987.95
BP-4 53.69% Φ_1 , 46.31% Φ_2	130	135	68.19	68.19	45	10^4	0.116	0.1	9.0	9.0	9.0	2.9	9.0	9.0	10^{-14}	1142.13	624.92	534.13	463.67	125.23	0.0028	1279.4	738.66	972.34
BP-5 52.03% Φ_1 , 47.97% Φ_2	130	140	62.95	62.95	45	10^4	0.11	0.11	9.0	9.0	9.0	2.9	9.0	9.0	10^{-14}	1150.57	635.59	578.61	481.12	124.23	0.0028	1279.4	738.66	972.34

TABLE I: *Extended scalar sector parameters (scalar field VEV's and quartic couplings λ 's) and the corresponding scalar masses in GeV for five representative benchmark points in this framework has been shown.*

IV. BENCHMARK POINTS OF THE MODEL

We now deliberate on the selected benchmark points shown in Table I that satisfy the various constraints discussed in the previous section. There are multiple parameters, VEV of the scalar fields (GeV), scalar quartic couplings λ 's (λ 's are $\lambda_{1a}, \lambda_{1b}, \lambda_{2a}, \lambda_{2b}, \lambda_3, \lambda_4, \lambda_5, \lambda_8$ and λ_s) that control the masses and the corresponding phenomenology of this scenario are shown in Table I.

We choose to assign these following values to the various other parameters in the model such as $\lambda_{4a} \approx 10^{-11}$ (the variation will be seen in the dark matter section later), the singlet scalar VEV $v_s \approx 10^4$ GeV, $\lambda_s = 10^{-15}$ and $y_{s\ell} \sim 10^{-8}$ to simultaneously obtain the neutrino mass in the correct order $m_\nu = \frac{y_{s\ell}^2 v_s^2}{M_{f_{MF}}} \approx 0.1$ eV and correct order of dark matter relic density through freeze-in mechanism. We choose the numerical values of the parameters (scalar quartic couplings, VEVs, etc.) in such a way that the second lightest (at tree-level) component \tilde{H} acts as the SM like Higgs boson. The dominant contribution from the doublet Φ_1 and Φ_2 to the Higgs like scalar is also shown in Table I. For these selections of the benchmark points, the mixing between the THDM like Higgs doublet ($\Phi_{1,2}$) and other scalar multiplets ($\Phi_{1M,2M}, \chi$) are very small, hence the $\mathcal{O}(300)$ GeV scalar masses are still allowed from the experimental constraints, as can be seen from the Table I. Note that all the quartic couplings (parameters of the scalar potential) have been varied within the perturbative range and charged SM *up-type* quarks, *down-type* quarks and charged mirror fermions and their right handed neutrinos get their masses due to the VEVs specified by v_1, v_2, v_{1M} and v_{2M} . We also see that for the choice of smaller values of other scalar VEVs v_{1M}, v_{2M} and v_M with quartic coupling $\mathcal{O}(1)$, the other CP-even and charged scalar fields masses become lesser or close to $M_{\tilde{H}} \approx 125$ GeV which is disfavored by the present LHC data [43, 44]. Assigning large values for these VEVs is disallowed as it is bounded by v_{SM} .

Furthermore, one can take the triplet scalar (both $\tilde{\chi}$ and ξ) VEV $v_M > 3$ GeV as there is no violation of custodial symmetry at tree-level in the presence of both hypercharge $Y = 0$ and $Y = 2$ triplet scalar fields. We choose the value for the VEV $v_M = 40$ GeV, hence by adjusting the mirror Yukawa coupling y_M (see eqn. A19) one can get the large neutral mirror lepton masses $\approx \frac{y_M v_M}{\sqrt{2}}$. We also choose the value of $y_{s\ell} \sim \mathcal{O}(10^{-8})$ and singlet scalar VEV $v_s = 10^4$ GeV to get the neutrino mass ~ 0.1 eV. We choose similar order VEVs for the other mirror scalar doublet $\Phi_{1M,2M}$ and adjusted the mirror Yukawa coupling $y_{\ell,d,u}^M$ to evade the EWPT, LFV, LHC signal strengths and other constraints. It is noted that the mixing between the SM and mirror fermions will not affect the masses of the fermions as the yukawa is $y_{s\ell} \sim \mathcal{O}(10^{-8})$. However, these small mixing can help to get the neutrino low energy variables: masses and mixing angles, dark matter density and may solve the strong-CP problems. These new mirror Yukawa coupling do not affect the scalar sector mass spectrum at tree-level, however it can alter the mass spectrum at loop-level depending on the parameters. In this present work, we only focus on the tree-level mass spectrum

as the radiative correction to the masses of the scalars and fermions is beyond the scope of this manuscript.

In this framework, the up-type and down-type quarks are coupled to two different THDM like scalar doublets and similar type of interactions are present in the mirror sector. This behavior is analogous to the Type-II 2HDM[45–47] in both sectors. The first THDM like doublet Φ_1 interacts with the SM charged leptons and down-type quarks whereas second THDM like doublet Φ_2 couples to the up-type quarks (see eqn. A19). Here, we assume that the Higgs-125 GeV scalar \tilde{H} is mostly generated from the real part of the doublets Φ_1 , and Φ_2 . Hence, the effect from the other scalar multiplets on the Higgs signal strength due to mixing can be taken to be negligible. The decay rate of \tilde{H} into two lightest CP-even scalar \tilde{H}_s (and two dark matter A_s^0) fields can contribute to the Higgs invisible decay width depending on mixing, i.e., the value of the quartic coupling λ_{4a} and the VEVs ($v_1, v_2, v_{1M}, v_{2M}, v_M$ and v_s) of the scalar fields. We have carefully chosen the values of these VEVs as can alter the mixing and masses of all the model particles. In particular, these VEVs can significantly modify the $\tilde{H}t\bar{t}$ coupling, hence affect the Higgs to gluon-gluon ($\tilde{H}gg$) coupling via top loop. This coupling strength would increase by κ_t , where $\kappa_t = \left(\frac{y_{t,\text{New}}}{y_{t,\text{SM}}}\right) \equiv \left(\frac{v_{\text{SM}}}{v_2} O_H^{52}\right)$, the ratio of the top Yukawa coupling for the \tilde{H} of this model relative to the SM value. The production cross-section of the Higgs-125 GeV will be different in this framework in comparison to the SM and can be expressed as $R_\sigma \equiv \frac{\sigma(pp \rightarrow \tilde{H})_{\text{BSM}}}{\sigma(pp \rightarrow h)_{\text{SM}}} \approx \frac{\sigma(gg \rightarrow \tilde{H})_{\text{BSM}}}{\sigma(gg \rightarrow h)_{\text{SM}}} \propto \kappa_t^2$. For our all benchmark points as shown in Table I, the mixing angle $O_H^{52} \approx 0.69$ and the minimization condition of the complete scalar potential implies that the individual value of both v_1 and v_2 must be smaller than v_{SM} . The combined effect of these two makes $R_\sigma > 1$, leading to enhanced production cross-section for the SM like \tilde{H} compared to that for the SM like Higgs boson. On the other hand, we know that $\mu_{\gamma\gamma}$ and $\mu_{WW,ZZ}$ are measured very precisely and provide the most stringent limit on the parameters of any BSM scalar decaying into those final states [42].

Hence, the enhancement in the production rate $gg \rightarrow \tilde{H}$ should be compensated by suppression of the branching ratio $BR(\tilde{H} \rightarrow xx)_{\text{BSM}}$, where $x = \gamma, W, Z$, so that μ_{xx} consistent with $(\mu_{xx})^{\text{exp}}$. We find that for our benchmark points (see Table I) the branching ratio $BR(\tilde{H} \rightarrow \gamma\gamma)$ is (5–18%) lower compared to SM-value (see Table II). Thus the model predicted $\mu_{\gamma\gamma}$ is consistent with the observed data [42]. It is noted that the other heavy charged-scalar particles through one-loop do not affect on these signal strength $\mu_{\gamma\gamma}$ due to the tiny quartic coupling λ_{4a} . On the other hand,

due to six custodial $SU(2)_D$ CP-even scalar mixing $BR(\tilde{H} \rightarrow WW, ZZ) \approx 15 - 30\% \times BR(\tilde{H} \rightarrow WW, ZZ)_{SM}$ and the corresponding Higgs (\tilde{H}) signal strengths $\mu_{WW,ZZ}$ for our choice of benchmark points remain within 1σ limit of $(\mu_{WW,ZZ})^{exp}$. Also noted that the quartic couplings λ_{4a} and λ_s are taken to be very small as the dark matter is non-thermally produced through these couplings. While investigating this, we also find that the particular VEVs $v_{1M} = v_{2M} \approx v_M \gtrsim 70$ GeV could violate the Higgs signal strength data due to the following reasons: (i) in this model, we have two additional (total four) scalar doublets and two triplets, hence $v_{SM} \equiv \sqrt{v_1^2 + v_{1M}^2 + v_2^2 + v_{2M}^2 + 8v_M^2} = 246$ GeV and (ii) the smallness of the two THDM like Higgs doublets VEVs v_1 or v_2 could increase the gluon-gluon (quark-quark-)Higgs like scalar coupling strength due to large Yukawa coupling $y_{u,d}$ compatible with quark masses while decreasing the Higgs to two gauge bosons coupling strength. For this choice of the parameters, the total decay width of the SM like Higgs boson becomes large (especially the $\Gamma(\tilde{H} \rightarrow b\bar{b}, \tau\bar{\tau})$), hence the branching of all the other channels get significantly altered which violate the Higgs signal strength data.

	Benchmark Points and Branching of SM like Higgs						
	$Br(\tilde{H} \rightarrow b\bar{b})$	$Br(\tilde{H} \rightarrow \tau\bar{\tau})$	$Br(\tilde{H} \rightarrow WW^*)$	$Br(\tilde{H} \rightarrow ZZ^*)$	$Br(\tilde{H} \rightarrow \gamma\gamma)$	$Br(\tilde{H} \rightarrow \tilde{H}_s\tilde{H}_s, A_s^0 A_s^0)$	$Br(\tilde{H} \rightarrow \text{Other BSM})$
SM	5.66×10^{-01}	6.21×10^{-02}	2.26×10^{-01}	2.81×10^{-02}	2.28×10^{-03}	—	—
BP-1	6.91×10^{-01}	8.56×10^{-02}	1.98×10^{-01}	2.46×10^{-02}	1.96×10^{-03}	$< 1 \times 10^{-06}$	$< 1 \times 10^{-06}$
BP-2	6.98×10^{-01}	8.64×10^{-02}	1.92×10^{-01}	2.38×10^{-02}	1.95×10^{-03}	$< 1 \times 10^{-06}$	$< 1 \times 10^{-06}$
BP-3	6.71×10^{-01}	8.31×10^{-02}	2.12×10^{-01}	2.63×10^{-02}	2.11×10^{-03}	$< 1 \times 10^{-06}$	$< 1 \times 10^{-06}$
BP-4	7.25×10^{-01}	8.98×10^{-02}	1.63×10^{-01}	2.02×10^{-02}	1.94×10^{-03}	$< 1 \times 10^{-06}$	$< 1 \times 10^{-06}$
BP-5	7.23×10^{-01}	8.95×10^{-02}	1.64×10^{-01}	2.03×10^{-02}	1.93×10^{-03}	$< 1 \times 10^{-06}$	$< 1 \times 10^{-06}$

TABLE II: *The Branching fraction of the SM Higgs and the 125 GeV \tilde{H} are shown for five benchmark points of Table. I.*

In Tables II we show the different branching ratios for \tilde{H} and also provide the corresponding values for the SM higgs boson for comparison. For our choice of benchmark points, the \tilde{H} branching ratios to various SM two body final states are consistent with that of the current LHC Higgs boson data. It should be also noted that the invisible decay of \tilde{H} is negligible small. We have presented the corresponding Higgs signal strengths in Table III.

As seen in Tables I and III, by choosing v_1 within $130 - 150$ GeV, we always obtain μ_{bb} and $\mu_{\tau\tau}$ avry between $1.42 - 2.06$ and $1.59 - 2.30$ respectively. This large value can be easily understood. Including the production rate, an additional increment come from the branching ratios of these

Signal Strength	Benchmark Points and Signal strength of SM like Higgs				
	$\mu_{b\bar{b}}$	$\mu_{\tau\bar{\tau}}$	μ_{WW}	μ_{ZZ}	$\mu_{\gamma\gamma}$
$\mu_{\text{Best-Fit}}$	$2.51^{+2.43}_{-2.01}$	$1.05^{+0.53}_{-0.47}$	$1.35^{+0.35}_{-0.21}$	$1.22^{+0.23}_{-0.21}$	$1.16^{+0.21}_{-0.18}$
$\mu_{\text{BP-1}}$	1.70	1.91	1.214	1.211	1.19
$\mu_{\text{BP-2}}$	1.81	2.03	1.239	1.236	1.25
$\mu_{\text{BP-3}}$	1.42	1.59	1.114	1.111	1.10
$\mu_{\text{BP-4}}$	1.85	2.06	1.03	1.029	1.23
$\mu_{\text{BP-5}}$	2.06	2.30	1.16	1.15	1.22

TABLE III: *125-GeV Higgs boson signal strengths for five benchmark points of Table. I. The experimental best fit $\mu_{\text{Best-Fit}}$ are the CMS combined measurements of the Higgs boson couplings at 13 TeV run of the LHC with 35.9 fb^{-1} data [42]. The error bars shown on $\mu_{\text{Best-Fit}}$ are at one sigma.*

two channels $\Gamma(\tilde{H} \rightarrow b\bar{b})$ and $\Gamma(\tilde{H} \rightarrow \tau\bar{\tau})$ due to the enhanced Higgs to two bottom quarks $\left(\frac{y_{b,\text{New}}}{y_{b,\text{SM}}}\right) \equiv \left(\frac{v_{\text{SM}}}{v_1} O_H^{51}\right)$ and Higgs to two tau leptons $\left(\frac{y_{\tau,\text{New}}}{y_{\tau,\text{SM}}}\right) \equiv \left(\frac{v_{\text{SM}}}{v_1} O_H^{51}\right)$ couplings. The mixing element of the $SU(2)_D$ CP-even singlet mass matrix is $O_H^{51} \approx 0.72$ for our choice of BPs. Here the combination of the mixing element O_H^{51} and ratio of VEVs $\frac{v_{\text{SM}}}{v_1}$ can increase the branching of $\Gamma(\tilde{H} \rightarrow b\bar{b})$ and $\Gamma(\tilde{H} \rightarrow \tau\bar{\tau})$ channels. The BPs with signal strengths $\mu_{bb,\tau\tau}$ are allowed by the present LHC signal strength data within 1 or 2σ [42] (see Table III for the SM Best-Fit data). It is noted that one could not decrease these branchings by changing the VEVs or quartic coupling resulting deviation of the Higgs-like \tilde{H} mass from ~ 125 GeV and other branchings $BR(\tilde{H} \rightarrow xx)$, where $x = \gamma, W, Z$.

V. SUB-MEV DARK MATTER OF THE MODEL

Let us now turn our attention to the possibility of accommodating a sub-MeV dark matter candidate in this framework. In this scenario, it is noted that the imaginary part of the complex singlet scalar does not mix with the other scalars and as a result can serve as a viable dark matter candidate $A_s^0 \equiv Im(\Phi_s)$. The transformation of the following fields can be expressed as $\Phi_{1,2} \rightarrow e^{-2i\alpha_{\text{SM}}} \Phi_{1,2}$, $\Phi_{1M,2M} \rightarrow e^{2i\alpha_{\text{MF}}} \Phi_{1M,2M}$, $\tilde{\chi} \rightarrow e^{-2i\alpha_{\text{MF}}} \tilde{\chi}$, $\xi \rightarrow \xi$ and $\Phi_s \rightarrow e^{-i(\alpha_{\text{SM}} + \alpha_{\text{MF}})} \Phi_s$.

The $\lambda_{5,6}$'s terms, in the potential (see eqn. A6), break the $U(1)_{\text{SM}} \times U(1)_{\text{MF}}$ symmetries explicitly. Total three ‘massless’ Nambu-Goldstone bosons can be obtained after spontaneous breaking of $SU(2)_L \times U(1)_Y \rightarrow U(1)_{em}$ by imposing the condition $\lambda_{5a} = \lambda_{5b} = \lambda_{6a} = \lambda_{6b} = \lambda_{7a} = \lambda_{7b} = \lambda_{7ab} = \lambda_{7aMb} = \lambda_{7abM} = \lambda_5$. Similarly the first line of λ_{5c} term in the potential (see eqn. A6) is $U(1)_{\text{SM}} \times U(1)_{\text{MF}}$ conserving, and the second line explicitly violates these symmetries. All these terms help to get exact minimization of the scalar potential. In the absence of the λ_{5c} term, one can always get an additional ‘massless’ neutral Nambu-Goldstone, i.e., the complex singlet type pseudoscalar (PSS) remain massless. The $U(1)_{\text{SM}} \times U(1)_{\text{MF}}$ breaking λ_{5c} terms help us to get non-zero sub-MeV mass for the singlet-type complex pseudoscalar field A_s^0 . At the tree-level the mass of the complex singlet scalar is given by

$$M_{A_s^0}^2 = 8 \lambda_{5c} (v_1 + v_2)(v_{1M} + v_{2M}). \quad (5.1)$$

For the chosen BPs, the numerical values of $(v_1 + v_2)(v_{1M} + v_{2M})$ remain almost same and the dark matter mass only depends on the quartic coupling λ_{5c} . The Higgs portal coupling ($A_s^0 A_s^0 \tilde{H}$) is also proportional to the coupling $\lambda_{5c}, \lambda_{4a}$ and VEVs (see the eqns. 6.17). In the following sections, we discuss the various bounds on the model parameter space [27, 37, 41, 48] coming from terrestrial and laboratory-base experiments.

Motivated by the possibility of a viable dark matter candidate in this scenario, we investigate the mass ranges and the corresponding stability conditions for the A_s^0 . If the dark matter is heavy, then it can decay into two fermions at tree-level and corresponding the decay width is given by

$$\Gamma(A_s^0 \rightarrow f\bar{f}) = \frac{N_f^c M_{A_s^0} y_f^2}{8\pi} \left(1 - \frac{4m_i^2}{M_{A_s^0}^2}\right)^{\frac{1}{2}}, \quad (5.2)$$

where, $y_f \approx \sqrt{2} \frac{y_{si}^2 v_s}{y_i^M v_{2M}}$, $i = u, d, \ell$ (see eqns A26 and A27) for $v_M = v_{1M} = v_{2M}$. One can also find the decay life time in this case as

$$\tau_{A_s^0} = \frac{6.5821 \times 10^{-25}}{\Gamma_{A_s^0}^{\text{Total}} \text{ [in GeV]}} \text{ seconds} \quad (5.3)$$

Here we use the natural unit conversion $1 \text{ GeV}^{-1} = 6.5821 \times 10^{-25}$ seconds. If $M_{A_s^0} > 2m_e$, it can decay only into two electrons. The stability of the DM demands that $\tau_{A_s^0} > \tau_U$ where, $\tau_U \approx 4.35 \times 10^{17}$ seconds is the lifetime of the Universe. For the chosen parameters, $M_{A_s^0} = 1.023 \text{ MeV}$,

$\left(\frac{v_{2M}}{v_s}\right)^2 = 1.848 \times 10^{-5}$ and $y_e^M \simeq \sqrt{4\pi}$, we find the limit on the coupling $y_{s\ell}$ to stabilize the dark matter

$$y_{s\ell} < 5.14091 \times 10^{-11}. \quad (5.4)$$

Furthermore, in the present framework, we are interested in the sub-MeV DM mass which is also

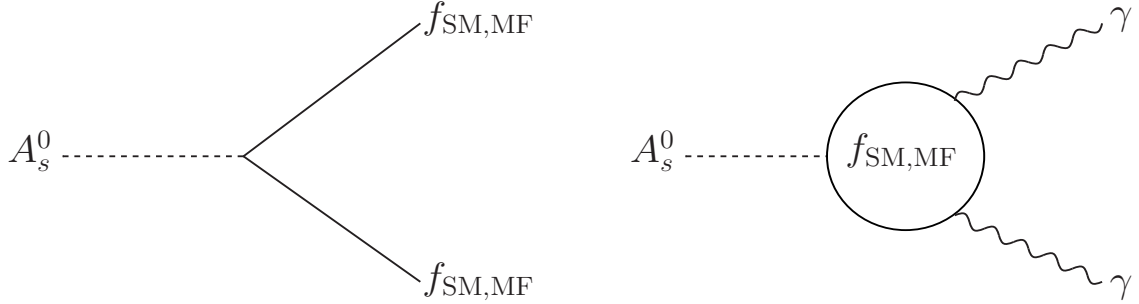


FIG. 1: Possible two body (tree- & one-loop) decay Feynman diagram of A_s^0 .

motivated from the theoretical framework. As the dark matter mass is light (sub-MeV), it is unable to decay into two fermions at tree-level, however there is a possibility of decaying into two photons through the SM and mirror charged particles (see Fig. 1). The decay width for the dark matter decaying into two photons is given by

$$\Gamma(A_s^0 \rightarrow \gamma\gamma) = \Gamma(A_s^0 \rightarrow \gamma\gamma)^{\text{SM fermions}} + \Gamma(A_s^0 \rightarrow \gamma\gamma)^{\text{MF fermions}}, \quad (5.5)$$

where,

$$\Gamma(A_s^0 \rightarrow \gamma\gamma)^{\text{SM fermions}} = \frac{\alpha^2 M_{A_s^0}^3}{256\pi^3 v_{\text{SM}}^2} \left| \sum_f N_f^c Q_f^2 y_f F_{1/2}(\chi_f) \right|^2 \quad (5.6)$$

$$\Gamma(A_s^0 \rightarrow \gamma\gamma)^{\text{MF fermions}} = \frac{\alpha^2 M_{A_s^0}^3}{256\pi^3 v_{\text{SM}}^2} \left| \sum_f N_f^c Q_f^2 y_f^M F_{1/2}(\chi_f) \right|^2, \quad (5.7)$$

here, $\chi_i = M_{A_s^0}^2/4m_i^2$. Q_f denotes electric charges of the corresponding particles. N_f^c is the color factor. In the limit $y_{sd} \approx y_{sq} \approx y_{su} = y_s$, $y_f = -y_f^M \approx \sqrt{2} \frac{y_{si}^2 v_s}{y_i^M v_{2M}}$ (see eqns A26 and A27) denote A_s^0 couplings to $f_i \bar{f}_i$ and $f_i^M \bar{f}_i^M$ where, $i = u, d, \ell$. The loop function $F_{1/2}$ is defined as

$$F_{1/2}(\chi) = 2[\chi + (\chi - 1)f(\chi)]\chi^{-2}, \quad (5.8)$$

where,

$$f(\chi) = \begin{cases} (\sin^{-1} \sqrt{\chi})^2, & \chi \leq 1 \\ -\frac{1}{4} [\ln \frac{1+\sqrt{1-\chi^{-1}}}{1-\sqrt{1-\chi^{-1}}} - i\pi]^2, & \chi > 1 \end{cases}, \quad (5.9)$$

As previously stated the corresponding couplings being $y_s < 0.1 y_{s\ell}$ [40, 41] to solve the strong CP problem in this framework, the decay $\Gamma(A_s^0 \rightarrow \gamma\gamma)$ channel through SM-quarks are suppressed. Additionally, as the mass of mirror-fermions are large ($\mathcal{O}(150)$ GeV), the decays through mirror-fermions are also small as compared to the other channels. It is to be noted that the coupling of A_s^0 with two charged scalars or charged gauge bosons are absent (protected from the $U(1)_{\text{SM}} \times U(1)_{\text{MF}}$ symmetries) in this model. As a result, the decay $\Gamma(A_s^0 \rightarrow \gamma\gamma)$ through the SM charged lepton loop becomes dominant one and gives rise to the most stringent bound on the coupling $y_{s\ell}$. Hence we obtain

$$\Gamma_{\text{tot}}(A_s^0 \rightarrow \gamma\gamma) = \frac{\alpha^2 M_{A_s^0}^3}{256\pi^3 v_{\text{SM}}^2} \frac{y_{s\ell}^4}{(y_{\ell}^M)^2} \frac{v_s^2}{v_{2M}^2} |F_{1/2}(\chi_e) + F_{1/2}(\chi_{\mu}) + F_{1/2}(\chi_{\tau})|^2. \quad (5.10)$$

The decay through electron loop is the dominant one as $F_{1/2}(\chi_e) \gg F_{1/2}(\chi_{\mu}) \gg F_{1/2}(\chi_{\tau})$ for $M_{A_s^0} \leq 1$ MeV. Hence

$$\Gamma_{\text{tot}}(A_s^0 \rightarrow \gamma\gamma) \approx \frac{\alpha^2 M_{A_s^0}^3}{256\pi^3 v_{\text{SM}}^2} \frac{y_{s\ell}^4}{(y_{\ell}^M)^2} \frac{v_s^2}{v_{2M}^2} |F_{1/2}(\chi_e)|^2 \quad (5.11)$$

and using this we can obtain the life-time of the pseudoscalar given by

$$\tau_{A_s^0} = \frac{6.582 \times 10^{-25}}{\Gamma_{\text{tot}}(A_s^0 \rightarrow \gamma\gamma) [\text{in GeV}]} \text{ seconds} \quad (5.12)$$

The dark matter stability condition imposes an upper limit on the couplings. Taking $\left(\frac{v_{2M}}{v_s}\right)^2 = 1.848 \times 10^{-5}$ and $(y_{\ell}^M)^2 \sim 4\pi$, the limit on $y_{s\ell}$ can be obtained as

$$\begin{aligned} y_{s\ell}^4 &\lesssim \frac{6.582 \times 10^{-25}}{\tau_U} \frac{256\pi^3 v_{\text{SM}}^2 (y_u^M)^2}{\alpha^2 M_{A_s^0}^3 |F_{1/2}(\chi_e)|^2} \left(\frac{v_{2M}}{v_s}\right)^2 \\ y_{s\ell} &\lesssim \frac{7.255 \times 10^{-9}}{M_{A_s^0}^{3/4} |F_{1/2}(\chi_e)|^{1/2}}. \end{aligned} \quad (5.13)$$

We get $|F_{1/2}(\chi_e)| = 1.922$ for $M_{A_s^0} = 1$ MeV and get the bound on $y_{s\ell}$

$$y_{s\ell} < 9.305 \times 10^{-7}. \quad (5.14)$$

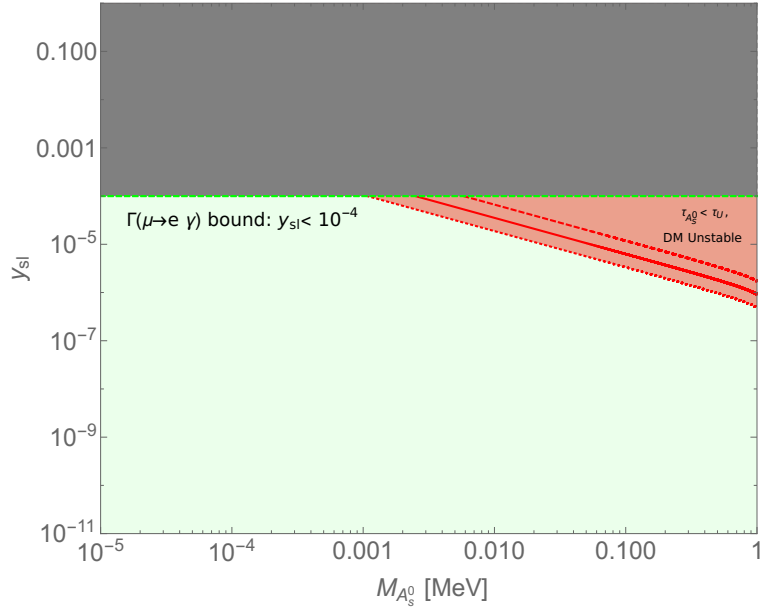


FIG. 2: Plot shows the exclusion region in $M_{A_s^0}$ – $y_{s\ell}$ plane. The dark matter is stable in the region below the red-line given by, $\tau_{A_s^0} > \tau_U$ where the three red lines correspond to $y_u^M = 1$ (dashed), $\sqrt{4\pi}$ (solid) and 4π (dotted) respectively. The gray-region is excluded from the $\mu \rightarrow e\gamma$ constraints and $\mu - e$ conversion [37] implying $y_{s\ell} < 10^{-4}$.

Similarly $|F_{1/2}(\chi_e)| = 1.33$ for $M_{A_s^0} = 1$ keV, hence

$$y_{s\ell} < 1.986 \times 10^{-4}. \quad (5.15)$$

The above analysis shows that the dark matter can remain stable for $y_{s\ell} \sim \mathcal{O}(10^{-2})$ for the mass ranges of keV and $y_{s\ell} \sim \mathcal{O}(10^{-5})$ and MeV scales respectively. It is to be noted that the parameter space is constrained by $\mu \rightarrow e\gamma$ and $\mu - e$ conversion implies $y_{s\ell} < 10^{-4}$ [37]. In Fig. 2, we present the allowed parameter space in $y_{s\ell} - M_{A_s^0}$ plane. The gray-region is excluded from the $\mu \rightarrow e\gamma$ decay and $\mu - e$ conversion constraints [37]. The direct detection limits [13] and indirect searches of the light dark matter may also put stringent constraints on the model parameter space which will be discussed in the later sections. It is to be noted that the direct detection limits [13] in this model for such light dark matter masses may not be applicable here. We plan to discuss the details of the relic density analysis (through the successful implementation of Freeze-in mechanism) in the upcoming section.

VI. FIMP-LIKE DARK MATTER DENSITY

From the previous discussion, it is established that the pseudoscalar singlet (PSS) A_s^0 can be a viable candidate for the dark matter, distributed in the Galactic halo. However, a decaying MeV scale dark matter candidate poses a viable limitation due to the fact that one has to implement fine-tuning [49, 50] to stabilize the dark matter as the lifetime of the DM particles has to be at least larger than the age of the Universe [51, 52]. The decay time of a particle is in general inversely proportional to its mass and proportional to the square of the couplings. In this model, we observe a viable, stable dark matter candidate in the interesting mass range of $\mathcal{O}(< 1)$ MeV with the corresponding quartic coupling related to the dark matter mass to be $\lambda_{5c} < \mathcal{O}(10^{-12})$. The most studied DM candidates are WIMPs that are thermally produced in the early universe with the relic density surviving after the Freeze-out. It is to be noted that the assumption behind the Freeze-out mechanism is that the coupling between the dark matter and SM particles cannot be too small; otherwise, it will never reach thermal equilibrium. Similarly, we cannot have large coupling for a small dark matter mass, as it will violate the perturbative-unitarity and the direct detection limits [13]. In this model, the dark matter dominantly annihilate (see Fig. 3) through

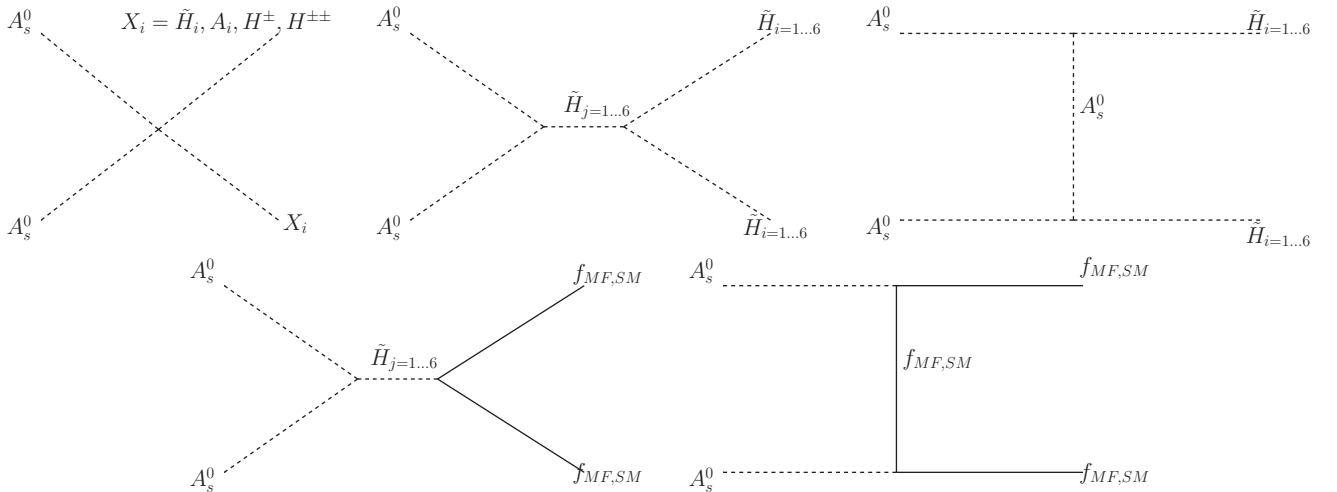


FIG. 3: *Dark matter annihilation diagrams contribute to the relic density through Freeze-out mechanism.*

the CP-even Higgses (\tilde{H}_{All}) and the corresponding Higgs portal couplings are shown in eqns. 6.17. For the dark matter mass we are interested in $\mathcal{O}(< 1)$ MeV, the allowed annihilation channels

are $A_s^0 A_s^0 \rightarrow \tilde{H}_{All} \rightarrow \bar{\nu}_\ell \nu_\ell$ and $A_s^0 A_s^0 \rightarrow \tilde{H}_{All} \rightarrow \bar{e} e$ (ν_ℓ is the three light neutrinos $\ell = e, \mu$ and τ) and other channels are kinematically forbidden with exception of the annihilation channels $A_s^0 A_s^0 \rightarrow \tilde{H}_{All} \rightarrow \bar{\nu}_\ell \nu_\ell$ only kinematically open to the dark matter mass $\mathcal{O}(< 0.5)$ MeV. The $A_s^0 A_s^0 \rightarrow \tilde{H}_{All} \rightarrow \gamma\gamma$ through charged Higgs in the loop are also kinematically allowed, however the contribution are negligibly small as compared to the other annihilation channels. The choice of these large Higgs portal and other couplings for the low dark matter mass $\mathcal{O}(< 1)$ MeV produces relic density at the right ballpark through the well established Freeze-out mechanism, but it violates the direct detection limits [13]. For example, we need a very large Higgs portal coupling $\lambda's = \mathcal{O}(500)$ (here $\lambda's$ are λ_{4a} , λ_{5c} and λ_s) for $M_{A_s^0} = 0.5$ MeV and $\lambda's = \mathcal{O}(1500)$ for $M_{A_s^0} = 100$ keV to get the thermally averaged annihilation cross-section $\sim 2.0 \times 10^{-26}$ cm³/s. This thermally averaged annihilation cross-section produce the relic density at right ball park $\Omega h^2 = 0.1198 \pm 0.0026$ [5]. The contribution to the direct detection cross-section can also come from interactions being mediated by CP-even Higgses (\tilde{H}_{All}) through t-channels $A_s^0 N \rightarrow A_s^0 N$ (N is the nucleus), hence being proportional to the square Higgs portal coupling. For large $\lambda's = \mathcal{O}(500 - 1500)$, we find the direct detection cross-sections are in the range $\sigma > 10^{-30}$ cm². These choices of Higgs portal couplings violate the direct detection experimental limit [13]. The large Higgs portal coupling also violates the perturbative-unitarity ($\lambda's \leq 4\pi$). Hence we find that the Freeze-out scenario is disfavored in this model for the dark matter mass we are interested in $< \mathcal{O}(1)$ MeV.

Let's now narrow our focus on why we are unable to obtain thermal dark matter in this framework. In Fig. 4, we present the decay rate for the mirror fermions to the dark matter and compared with the expansion rate of our universe. One can clearly see that those decays can thermalize dark matter in the early universe even for very small $y_{s\ell}$. One important point to remind the reader here is that we are considering the MeV scale DM. However, it can not remain in thermal bath for such low temperature as cosmological observations, in particular Big Bang Nucleosynthesis (BBN), will not allow one more degrees of freedom in the thermal bath at temperature $\mathcal{O}(\text{MeV})$. So, it has to decouple from the thermal bath at some higher temperature and for such relativistic decoupling, the relic density can be calculated by following [53]

$$\Omega h^2 = 7.83 \times 10^4 \left(\frac{g_i}{g_{*s}(T_{\text{dec}})} \left(\frac{M_{DM}}{\text{MeV}} \right) \right), \quad (6.1)$$

where, g_i is the internal degrees of freedom of DM, g_{*s} is the effective relativistic degrees of freedom

and T_{dec} is the decoupling temperature of DM. So, for MeV scale DM, it will be overproduced by few orders of magnitude compared to the present DM abundance.

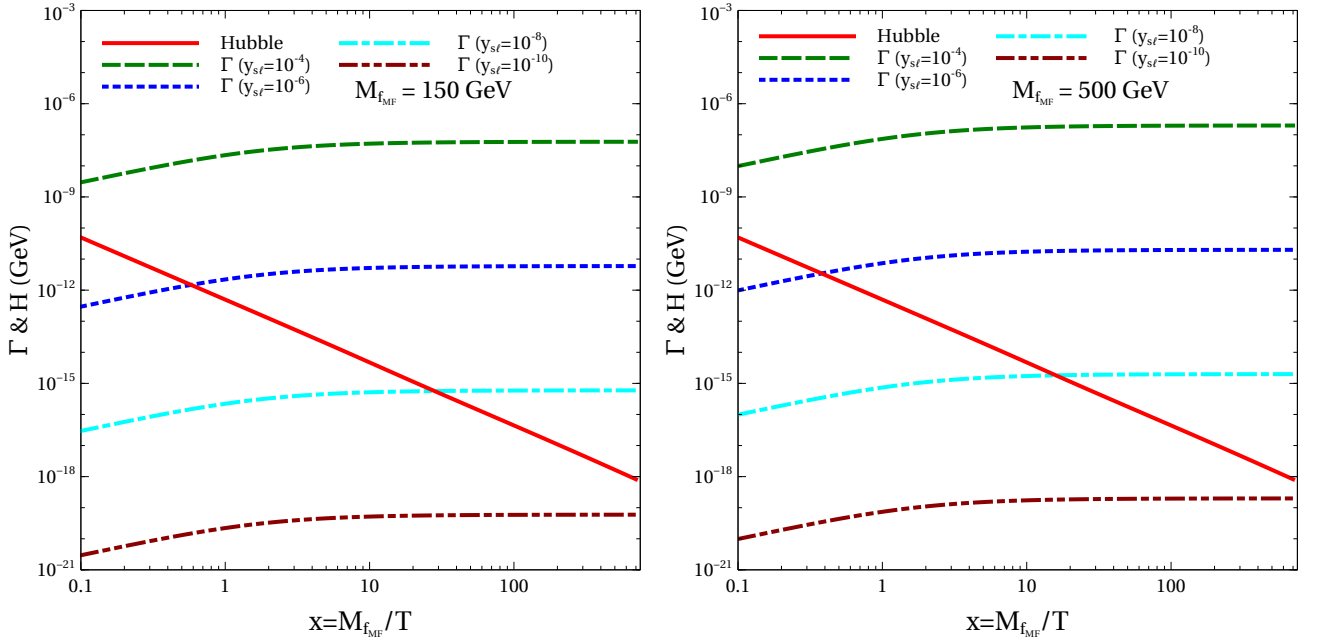


FIG. 4: The decay rates (Γ) of heavy mirror fermions to dark matter and SM neutrino are shown here for different benchmark values of $y_{s\ell}$ and mirror fermion masses 150 GeV (left-panel) and 500 GeV (right-panel). The red line stands for the Hubble expansion rate (H) of the universe as a function temperature T .

Hence we have established that in this framework it is not viable to have thermal dark matter and turn to the altrenative-a non-thermal dark matter scenario. We find that the non-thermally produced PSS can serve as a viable $\mathcal{O}(< 1)$ MeV (depending on the parameters $\lambda_{5c}, \lambda_{4a}, \lambda_s, y_s, y_{s\ell}$ and VEVs, see the Appendix A) dark matter candidate satisfying the dark matter relic density constraints. As the dark matter can interact with other particles very weakly (feebly), for such very weakly interacting particles, called feebly interacting massive particles or FIMPs, we can invoke the non-thermal, so-called Freeze-in mechanism. This mechanism needs feeble interactions which could be one of the reasons to have a aforementioned tiny couplings present in this model. The idea we pursue is that the dark matter sector gets populated through decay or annihilation of other heavy particle until the number density of the corresponding heavy particles species becomes Boltzmann-suppressed. For this, we need to solve Boltzmann equation that dictates the final relic

abundance for the dark matter candidate A_s^0 . The production of dark matter resulting from the decay of any mother particle (\tilde{H}_i ($i = 1,..6$), f_{MF}) is in thermal equilibrium at early universe. This condition is given by

$$\frac{\Gamma}{H} \geq 1, \quad (6.2)$$

where, Γ is the relevant decay width and H is the Hubble parameter given by [18, 54, 55]

$$H(T) = \left(g^* \frac{\pi^2}{90} \frac{T^4}{M_{\text{Pl}}^2} \right)^{1/2}, \quad (6.3)$$

where, $M_{\text{Pl}} = 1.2 \times 10^{19}$ GeV is the Planck mass. T is the temperature (1 GeV = 1.16×10^{13} Kelvin). If the production of mother particles occur mainly from the annihilation of other particles in the

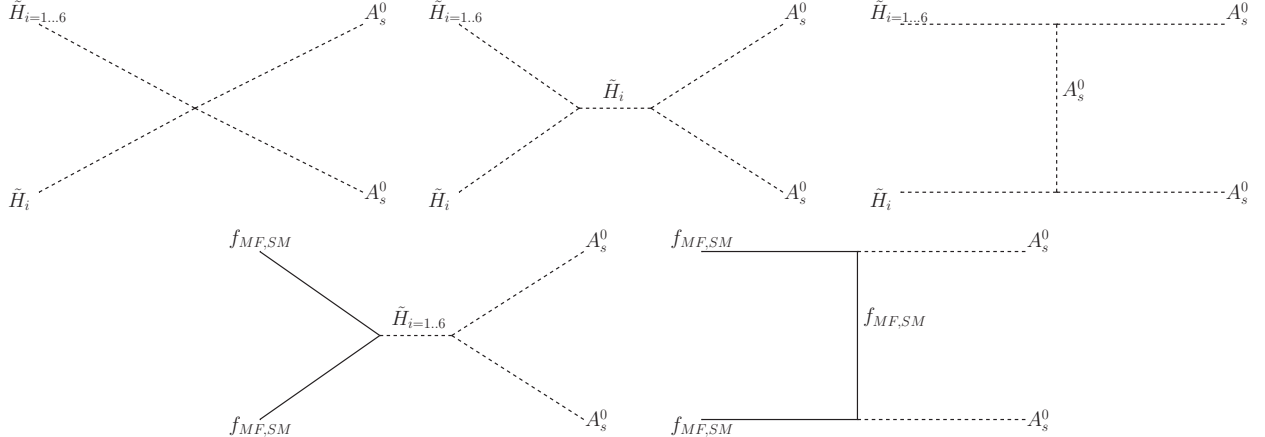


FIG. 5: *Annihilation-production diagrams for the dark matter from the Higgs, SM and mirror fermion.*

thermal bath Γ will be replaced by [18, 54, 55]

$$\Gamma = n_{eq} \langle \sigma v \rangle, \quad (6.4)$$

where n_{eq} is their equilibrium number density and is given by [54]

$$n_{eq} = \begin{cases} g^* \left(\frac{M T}{2\pi} \right)^{3/2} e^{-M/T}, & \text{for non-relativistic states } T \ll M \\ \frac{\zeta_3}{\pi^2} g^* T^3, & \text{for relativistic boson states } T \gg M \\ \frac{3}{4} \frac{\zeta_3}{\pi^2} g^* T^3, & \text{for relativistic fermion states } T \gg M \end{cases} \quad (6.5)$$

where the Riemann zeta function has the value $\zeta_3 = 1.2$ and $g^* = 208.5$ (for $T \gg M$) is the effective degrees of freedom in this framework and M stands for the mass of the particle. Here $\langle \sigma v \rangle$ is the thermally averaged annihilation cross-section for the particles in the thermal bath and can be written as [54, 56]

$$\langle \sigma_{xx} v \rangle = \frac{2\pi^2 T \int_{4M^2}^{\infty} ds \sqrt{s} (s - 4M^2) K_1\left(\frac{\sqrt{s}}{T}\right) \sigma_{xx}}{\left(4\pi M^2 T K_2\left(\frac{M}{T}\right)\right)^2}, \quad (6.6)$$

where σ_{xx} is the production annihilation cross-section of the mother particles ($x = \tilde{H}_{i=1..6}, f_{MF}$) from other particles in the thermal bath (see the production annihilation diagrams in Fig. 5) and $K_{1,2}$ is the modified Bessel function of functions of order 1 and 2 respectively.

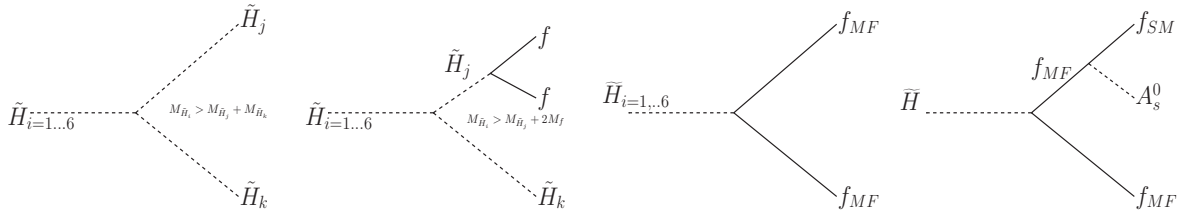


FIG. 6: *Decay diagrams contributing to the relic density. Decay-production diagrams for the heavy Higgs and mirror fermion help in thermal equilibrium in the early universe.*

In this scenario, we present various possible decays (see Fig. 6) and annihilation (see Fig. 7) production diagrams for the heavy Higgs and mirror fermions that facilitate in the thermal equilibrium in the early universe. There are other diagrams that can also contribute in the production of the heavy Higgs and mirror fermions. One can easily find that the Hubble parameter at early universe (temperature ~ 3000 Kelvin) $H(T) = 2.6 \times 10^{-38}$ GeV and the 2 and 3 body decay width for the heavy Higgs (\tilde{H}_i) are given by

$$\Gamma(\tilde{H}_i \rightarrow f_{MF} f_{MF}) = \frac{M_{\tilde{H}_i} y_M^2}{8\pi} \left(1 - 4 \frac{M_{MF}^2}{M_{\tilde{H}_i}^2}\right)^{3/2} \quad (6.7)$$

$$\Gamma(\tilde{H}_i \rightarrow \tilde{H}_j \tilde{H}_k) = \frac{y_{\tilde{H}_i \tilde{H}_j \tilde{H}_k}^2}{16\pi M_{\tilde{H}_i}^3} \left((M_{\tilde{H}_i}^2 - M_{\tilde{H}_j}^2 - M_{\tilde{H}_k}^2)^2 - 4 M_{\tilde{H}_j}^2 M_{\tilde{H}_k}^2\right)^{1/2} \quad (6.8)$$

$$\Gamma(\tilde{H} \rightarrow f_{MF} f_{SM} A_s^0) = \frac{1}{2\pi^3} \frac{1}{32M_{\tilde{H}}^3} |\mathcal{M}|^2 dE_1 dE_3, \quad \text{where, } |\mathcal{M}|^2 \propto \frac{y_M^2 y_{s\ell}^2}{M_{MF}^2}. \quad (6.9)$$

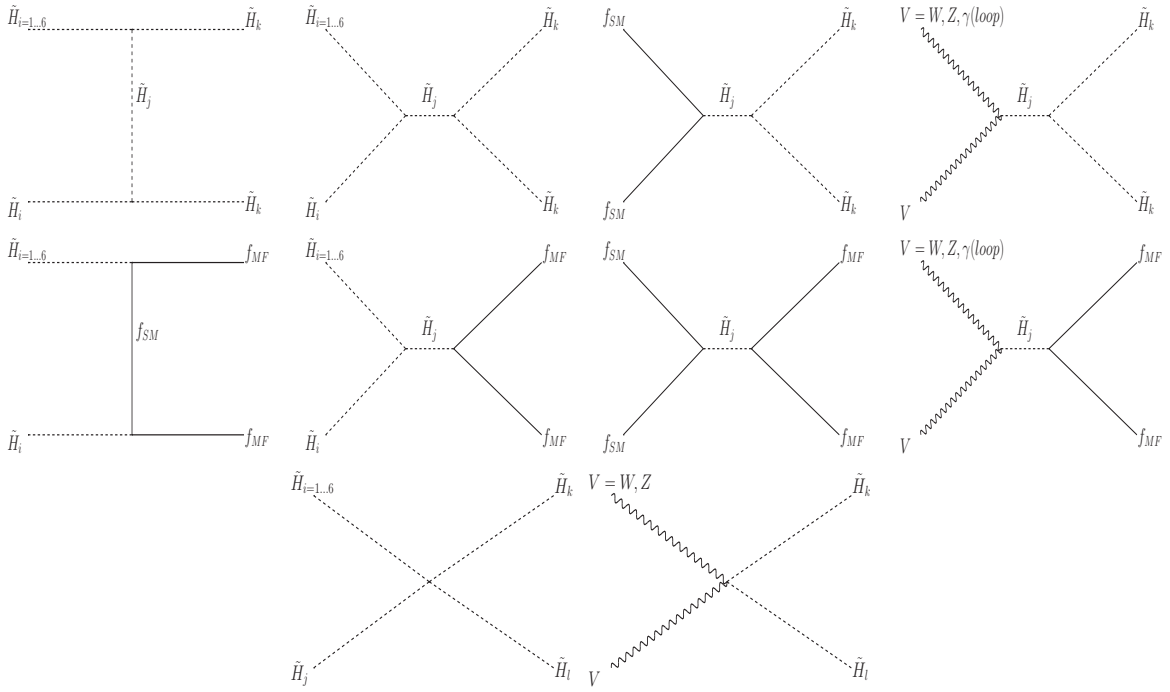


FIG. 7: *Annihilation-production diagrams for the heavy Higgs and mirror fermions help in thermal equilibrium in the early universe. It is to be noted that there are many other similar diagrams that can contribute in the production of the heavy Higgs and mirror fermions.*

Here $E_{1,2,3}$ are the energies of the final state particle for three-body decay [57]. We follow the Ref. [58] to calculate the three body decay widths and find the three-body decay rates to be always suppressed by additional propagator mass M_{MF}^2 and the coupling y_{si}^2 . It is to be noted that it is not challenging to obtain $\frac{\Gamma}{H} \gg 1$ due to the large decay width of the heavy particles in the early universe, resulting the heavy fermions being in thermal equilibrium with the thermal bath particles. Also to note that the lighter CP-even Higgs could also be produced from the decay of the heavier CP-even Higgs and the corresponding decay width is $\mathcal{O}(10)$ GeV. In this case we also find that $\frac{\Gamma}{H} \gg 1$. Hence the lighter lighter CP-even Higgs will also remain in thermal equilibrium with the thermal bath particles.

Similarly the scattering diagrams shown in Fig. 7 also provide $\frac{n_{eq} \langle \sigma v \rangle}{H} \gg 1$ in the model parameter space we are interested in. In this model, the dark matter can be produced from the decay of the mirror fermions, heavy scalars and from the annihilation of the other particles. It has already been discussed in existing literatures [18, 55, 59–68] that if same couplings are involved in

both decays as well as scattering processes then the former has the dominant contribution to DM relic density over the latter one.

Considering all these investigations, we take into account that the dark matter candidate is stable and can be produced only from the decay of the mirror fermions and heavy Higgses in this framework. The Boltzmann equation for the dark matter can be written as [18, 54, 55]

$$\frac{dn}{dt} + 3Hn = - \sum_i S(X_{Heavy,i} \rightarrow A_s^0 A_s^0, f_{SM} A_s^0), \quad (6.10)$$

where $X_{Heavy,i} = \tilde{H}_{i=1..6}$ ($\tilde{H}_{i=1..6}$ stand for the six physical CP-even mass eigenstates \tilde{H}'''' , \tilde{H}''' , \tilde{H}'' , \tilde{H}' , \tilde{H} , and \tilde{H}_s), f_{MF} and f_{SM} is SM fermions. Here the decay-based source term S can be written as

$$S = \Gamma(X_{Heavy,i} \rightarrow A_s^0 A_s^0, f_{SM} A_s^0) \frac{K_1(\frac{m_{X_{Heavy,i}}}{T})}{K_2(\frac{m_{X_{Heavy,i}}}{T})} n_{Heavy,i}^{eq} \quad (6.11)$$

where $K_{1,2}$ is the modified Bessel function of the first and second kind. For $x = \frac{m_{X_{Heavy,i}}}{T}$ and $Y = \frac{n}{T^3}$, the eqn. 6.10 now reads [54]

$$\frac{dY(x)}{dx} = \sum_i \frac{g_{X_{Heavy,i}}}{2\pi^2} \frac{\Gamma(X_{Heavy,i} \rightarrow A_s^0 A_s^0, f_{SM} A_s^0)}{H(x \approx 1)} x^3 K_1(x), \quad (6.12)$$

where $g_{X_{Heavy,i}}$ is the degrees of freedom of the heavy particle. We can integrate the dark matter production over the entire thermal history and find the final yield $Y(x_0)$ with the help of the appropriate integral [18, 54, 55]

$$Y(x_0) = \frac{45M_{Pl}}{6.64\pi^4 g_*^S \sqrt{g^\rho}} \sum_i \frac{g_{X_{Heavy,i}}}{M_{X_{Heavy,i}}^2} \Gamma(X_{Heavy,i} \rightarrow A_s^0 A_s^0, f_{SM} A_s^0) \int_0^\infty x^3 K_1(x) dx \quad (6.13)$$

g_*^S and g^ρ are the effective relativistic of degrees of freedom for the entropy density and energy density respectively. The relic density now can be written as [18, 54, 55]

$$\begin{aligned} \Omega h^2 &= \frac{h^2}{3H_0^2 M_{Pl}^2} \frac{M_{A_s^0}}{28} T_0^3 Y(x_0) \\ &\approx 1.09 \times 10^{27} M_{A_s^0} \sum_i \frac{g_{X_{Heavy,i}} \Gamma(X_{Heavy,i} \rightarrow A_s^0 A_s^0, f_{SM} A_s^0)}{M_{X_{Heavy,i}}^2} \end{aligned} \quad (6.14)$$

We now use eqn. 6.14 to calculate the relic density in this scenario. The main production diagrams from the decay widths of the heavy particles are shown in Fig. 8. The partial decay of

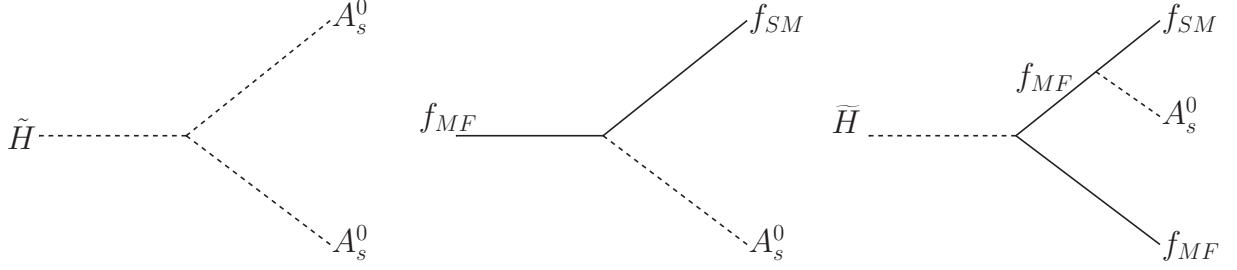


FIG. 8: *Dark matter production diagrams from the decay of the heavy particles contributing to the relic density.*

the heavy Higgs into the pair of dark matter and mirror fermion into SM fermion and a single dark matter are given by

$$\Gamma(\tilde{H}_i \rightarrow A_s^0 A_s^0) = \frac{y_{\tilde{H}_i A_s^0 A_s^0}^2}{32\pi M_{\tilde{H}_i}} \left(1 - \frac{M_{A_s^0}^2}{M_{\tilde{H}_i}^2}\right)^{\frac{1}{2}} \quad (6.15)$$

$$\Gamma(f_{MF} \rightarrow f_{SM} A_s^0) = \frac{M_{f_{MF}}}{8\pi} y_{f_{MF} f_{SM} A_s^0}^2. \quad (6.16)$$

with the corresponding coupling strengths given in terms of the mixing angles in the scalar sector (see eqns. A6-A15)

$$\begin{aligned} y_{\tilde{H}_s A_s^0 A_s^0} &= O_H^{61} y_{H_1^0 A_s^0 A_s^0} + O_H^{62} y_{H_2^0 A_s^0 A_s^0} + O_H^{63} y_{H_{1M}^0 A_s^0 A_s^0} + O_H^{64} y_{H_{2M}^0 A_s^0 A_s^0} + O_H^{65} y_{H_s^0 A_s^0 A_s^0}, \\ y_{\tilde{H} A_s^0 A_s^0} &= O_H^{51} y_{H_1^0 A_s^0 A_s^0} + O_H^{52} y_{H_2^0 A_s^0 A_s^0} + O_H^{53} y_{H_{1M}^0 A_s^0 A_s^0} + O_H^{54} y_{H_{2M}^0 A_s^0 A_s^0} + O_H^{55} y_{H_s^0 A_s^0 A_s^0}, \\ y_{\tilde{H}' A_s^0 A_s^0} &= O_H^{41} y_{H_1^0 A_s^0 A_s^0} + O_H^{42} y_{H_2^0 A_s^0 A_s^0} + O_H^{43} y_{H_{1M}^0 A_s^0 A_s^0} + O_H^{44} y_{H_{2M}^0 A_s^0 A_s^0} + O_H^{45} y_{H_s^0 A_s^0 A_s^0}, \\ y_{\tilde{H}'' A_s^0 A_s^0} &= O_H^{31} y_{H_1^0 A_s^0 A_s^0} + O_H^{32} y_{H_2^0 A_s^0 A_s^0} + O_H^{33} y_{H_{1M}^0 A_s^0 A_s^0} + O_H^{34} y_{H_{2M}^0 A_s^0 A_s^0} + O_H^{35} y_{H_s^0 A_s^0 A_s^0}, \quad (6.17) \\ y_{\tilde{H}''' A_s^0 A_s^0} &= O_H^{21} y_{H_1^0 A_s^0 A_s^0} + O_H^{22} y_{H_2^0 A_s^0 A_s^0} + O_H^{23} y_{H_{1M}^0 A_s^0 A_s^0} + O_H^{24} y_{H_{2M}^0 A_s^0 A_s^0} + O_H^{25} y_{H_s^0 A_s^0 A_s^0}, \\ y_{\tilde{H}'''' A_s^0 A_s^0} &= O_H^{11} y_{H_1^0 A_s^0 A_s^0} + O_H^{12} y_{H_2^0 A_s^0 A_s^0} + O_H^{13} y_{H_{1M}^0 A_s^0 A_s^0} + O_H^{14} y_{H_{2M}^0 A_s^0 A_s^0} + O_H^{15} y_{H_s^0 A_s^0 A_s^0}, \\ y_{\tilde{H}_i \tilde{H}_i A_s^0 A_s^0} &= \lambda_{4a}, \quad y_{f_{MF} f_{SM} A_s^0} = y_s \text{ (f is quark), } y_{s\ell} \text{ (f is lepton),} \end{aligned}$$

where,

$$\begin{aligned}
y_{H_1^0 A_s^0 A_s^0} &= \lambda_{4a} v_1 + 2\lambda_{5c} v_{1M} + 2\lambda_{5c} v_{2M}, \\
y_{H_2^0 A_s^0 A_s^0} &= 2\lambda_{5c} v_{1M} + \lambda_{4a} v_2 + 2\lambda_{5c} v_{2M}, \\
y_{H_{1M}^0 A_s^0 A_s^0} &= 2\lambda_{5c} v_1 + \lambda_{4a} v_{1M} + 2\lambda_{5c} v_2, \\
y_{H_{2M}^0 A_s^0 A_s^0} &= 2\lambda_{5c} v_1 + 2\lambda_{5c} v_2 + \lambda_{4a} v_{2M}, \\
y_{H_s^0 A_s^0 A_s^0} &= 2\lambda_s v_s, \quad y_{H_1^{0'} A_s^0 A_s^0} = 0.
\end{aligned} \tag{6.18}$$

where H_1^0 , H_2^0 , H_{1M}^0 , H_{2M}^0 , H_s^0 and $H_1^{0'}$ is the unphysical scalar fields (before mixing, see the Appendix A for details). The CP-even scalar incorporating both the triplet scalars $H_1^{0'} = \sqrt{\frac{2}{3}}\chi^{0r} + \sqrt{\frac{1}{3}}\zeta^0$ does not have the direct coupling to PSS dark matter, i.e., $y_{H_1^{0'} A_s^0 A_s^0} = 0$. The other scalars are unable to decay to PSS dark matter due to conservation of the $U(1)_{\text{SM}} \times U(1)_{\text{MF}}$ symmetry, charge, etc. Hence the initial DM density for the decay scenario mainly depends on the decay of these CP-even scalars and mirror fermions. One can see from these eqns. 6.17 and 6.18 that the decay of these heavy (physical) scalar fields and mirror fermions can be controlled by the λ_{5c} , λ_{4a} , λ_s , y_s , $y_{s\ell}$ and VEVs with the mass of the dark matter mainly depending on the λ_{5c} and VEVs (see eqn. 5.1).

As an example, let us first neglect the contribution from the decay of the mirror fermions $f_{MF} \rightarrow f_{SMA_s^0}$ (we consider $y_{s\ell} \ll 10^{-9}$) and consider the benchmark point BP-3 (see Table I). We choose $\lambda_s = 10^{-15}$, hence the lightest CP-even scalar field could not decay into the dark matter ($M_{\tilde{H}_s} < 2M_{A_s^0}$). The other CP-even state including 125 GeV scalar fields could decay into the dark matter which increases the abundance of the dark matter. Using BP-3 and $\lambda_{5c} = 3.2 \times 10^{-12}$ and $\lambda_{4a} = 7.377 \times 10^{-9}$, we obtain the dark matter mass as $M_{A_s^0} = 0.808$ MeV and find the numerical values of the coupling strengths $y_{\tilde{H}_s A_s^0 A_s^0} = 1.630 \times 10^{-11}$, $y_{\tilde{H} A_s^0 A_s^0} = -1.021 \times 10^{-6}$, $y_{\tilde{H}' A_s^0 A_s^0} = 3.390 \times 10^{-6}$, $y_{\tilde{H}'' A_s^0 A_s^0} = 1.059 \times 10^{-21}$, $y_{\tilde{H}''' A_s^0 A_s^0} = -9.424 \times 10^{-6}$ and $y_{\tilde{H}'''' A_s^0 A_s^0} = 3.669 \times 10^{-6}$. Finally, we obtain the relic density to be $\Omega h^2 = 0.1198$. We show the variation of the parameters λ_{5c} and λ_{4a} in Fig. 9(left) and similarly show the dark matter mass against λ_{4a} variation in Fig. 9(right). In both plots the red solid line represents $\Omega h^2 = 0.1198$ and the dashed red lines correspond to the 3σ variation in Ωh^2 with the darker region corresponding to the lower values of Ωh^2 .

We find that if we neglect the contribution from the scalar fields, the dark matter abundance could increase from the decay of the mirror fermions $f_{MF} \rightarrow f_{SMA_s^0}$. In this case, the contribution

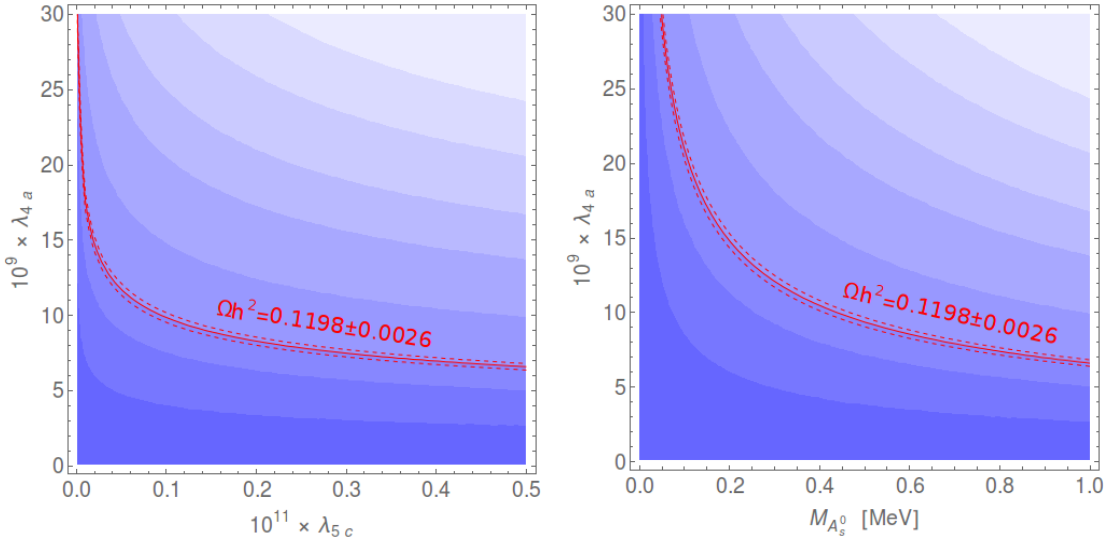


FIG. 9: *Plots show the variation of parameters λ_{5c} and λ_{4a} in left panel and similarly show the dark matter mass against λ_{4a} variation in right panel. These plots are generated for BP-3 as in Table I. In both plots the red solid line represents $\Omega h^2 = 0.1198$ and the dashed red lines correspond to the 3σ variation in Ωh^2 . The lighter region corresponds to higher values of Ωh^2 . For both these plots the contribution from the mirror fermion decay $f_{MF} \rightarrow f_{SM} A_s^0$ is sub-dominant and has been neglected.*

from the mirror quarks will also be negligibly small; as the corresponding Yukawa couplings are very small ($y_s \sim y_{sq} \sim y_{su} \sim y_{sd} < 0.1 y_{s\ell}$ [40, 41]). We obtain the relic density in the right ballpark for $y_{s\ell} \sim 4.428 \times 10^{-9}$ for $M_{A_s^0} = 10$ keV and $y_{s\ell} \sim 4.429 \times 10^{-10}$ with $M_{A_s^0} = 1$ MeV. The variation of dark matter mass against $y_{s\ell}$ is shown in Fig. 10. The blue dashed line indicates the 3σ relic density $\Omega h^2 = 0.1198 \pm 0.0026$ band [5]. The line above this blue line will overclose the Universe. The indirect detection bounds from HEAO and INTEGRAL experiments will be discussed in the section VII.

We now consider all these aforementioned contributions in the relic density calculation. The larger λ_{4a} increases the contributions from the heavy Higgs decays whereas large values of $y_{s\ell}$ increases the contributions from the mirror fermions. We present such variations for two different dark matter masses $M_{A_s^0} = 10$ keV and 0.5 MeV respectively in Fig. 11. The contribution is almost equal for $\lambda_{4a} \sim 4.90 \times 10^{-8}$ and $y_{s\ell} \sim 2.98 \times 10^{-9}$ with dark matter mass $M_{A_s^0} = 10$ keV and similarly for $\lambda_{4a} \sim 7.447 \times 10^{-9}$ and $y_{s\ell} \sim 3.78 \times 10^{-10}$ with dark matter mass $M_{A_s^0} = 0.5$ MeV. The dark

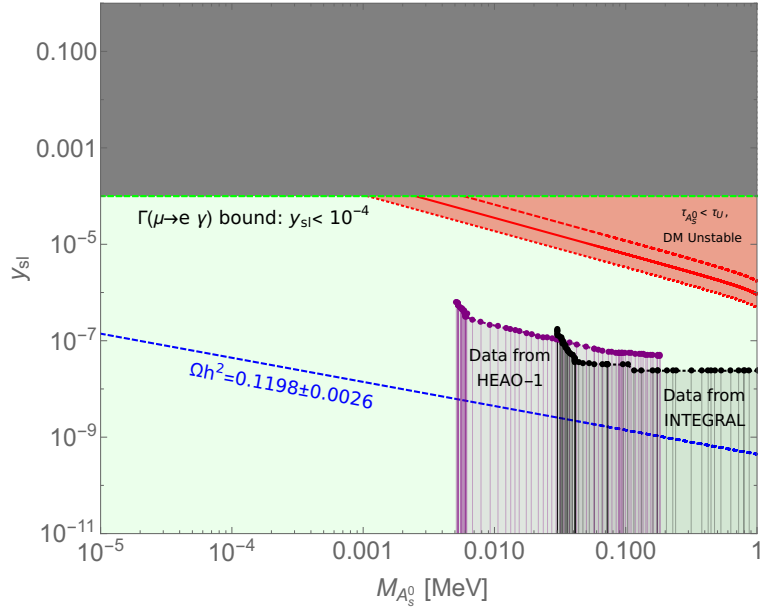


FIG. 10: *The same y_{sl} – $M_{A_s^0}$ plot as in Fig. 2 showing the relic density constraint and including the indirect detection bounds applicable in the parameter space. The blue dashed line indicates the relic density 3σ band $\Omega h^2 = 0.1198 \pm 0.0026$, and the constraints coming from the HEAO-1 [69] and INTEGRAL [70] indirect detection experiments.*

matter abundance increases as a result of the decay of the mirror fermions $f_{MF} \rightarrow f_{SM} A_s^0$. In this case, the contribution from the mirror quarks are negligibly small as $y_s \sim y_{sq} \sim y_{su} \sim y_{sd} < 0.1 y_{sl}$ [40, 41]. We also show the evolution of the dark matter with the temperature of the Universe in Fig. 12 for the following parameters: $\lambda_s = 10^{-15}$, $\lambda_{4a} \sim 4.90 \times 10^{-8}$ and $y_{sl} \sim 2.98 \times 10^{-9}$ and $M_{A_s^0} = 10$ keV. The plot clearly represents the significance of the Freeze-in mechanism in this framework, i.e., the initial DM density being zero and increasing during the cooling of the Universe. After a certain temperature ($T \sim \mathcal{O}(100)$ GeV) as shown in Fig. 12) the dark matter density becomes constant.

We have also looked into the bound from the free streaming length l_{fs} which will denote whether the dark matter will behave as hot, warm or cold. The $l_{fs} > 2$ Mpc region stands for hot dark matter region and can create challenges for the structure formation [71]. We avoid these regions (dark matter mass $\ll 1$ keV) in this analysis and calculate the free streaming length [72] for the dark matter with mass range keV up to MeV and find it to be consistently less than 10 kpc in the

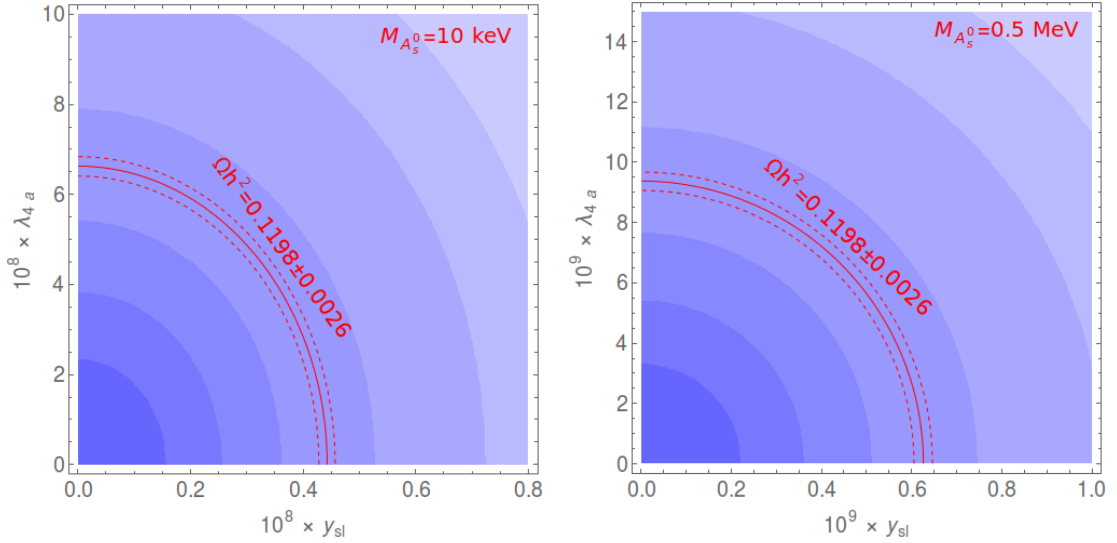


FIG. 11: *Plots show the variation of parameters λ_{4a} and y_{sl} for two different dark matter masses $M_{A_s^0} = 10$ keV (left) and 0.5 MeV (right). These plots are also generated for BP-3 as in Table I. In both plots the red solid line represents $\Omega h^2 = 0.1198$ and the dashed red lines correspond to the 3σ variation in Ωh^2 . The lighter region corresponds to higher values of Ωh^2 .*

parameter space referred to in the plots of Fig. 10. Hence we conclude that in this scenario A_s^0 behaves as a cold dark matter candidate [71].

In summary, in this section we have discussed the Freeze-in scenario for the dark matter candidate in this model and have already discussed the stability bound on the dark matter in the previous section. Now as we already know that the galactic and extra-galactic diffuse $X-ray$ or $\gamma-ray$ may come from the decay or annihilation of a dark matter through the loop which can put stringent constraints on the model parameter spaces of any dark matter model [73], in the next section we devote a discussion on the possible additional bounds coming from the available data from various indirect dark matter search experiments as well as direct detection experiments.

VII. INDIRECT AND DIRECT DETECTION OF DARK MATTER

Let us now focus on the detection possibilities of dark matter in our framework. One very interesting method is to look for some excess of photon or charged particles from different directions of our sky which may come from the annihilation or the decay of dark matter particles. The dark

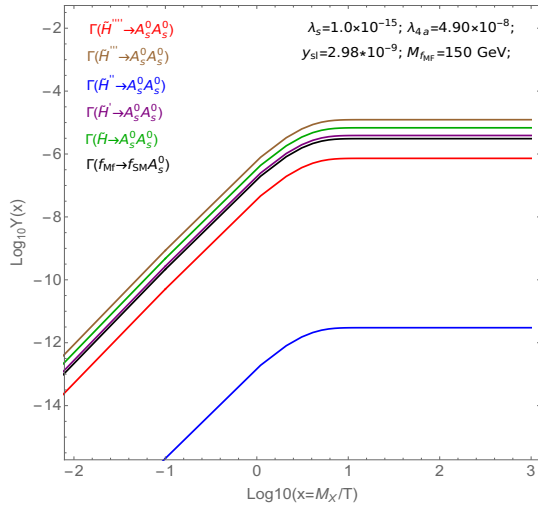


FIG. 12: Plot shows the variation of the yield $Y(x)$ against x for all the contribution coming from the heavy Higgs and mirror fermion decays. The Freeze-in mechanism effect can be clearly seen as the initial DM density is zero and increases during the cooling of the Universe and attaining a constant value after a certain temperature. We have scaled the mirror fermion decay contribution (black line) by a factor $1/10$ to distinguish from the others and used $M_X = 100$ GeV mass scale factor.

matter decay is less constrained from the early Universe cosmology. The galactic and extra-galactic diffuse $X - ray$ or $\gamma - ray$ background put the most stringent bounds on the model parameters of decaying DM [73]. The observations of the Fermi Large Area Telescope (Fermi-LAT) put limits on the weak-scale DM (mass $\mathcal{O}(100)$ MeV), having decay lifetime $\tau_{A_s^0} > 10^{26}$ s, many orders of magnitude larger than the age of the Universe [74, 75]. The usual gamma-ray constraints from the Fermi-LAT do not apply for the masses $< \mathcal{O}(100)$ MeV. However, the instruments in the several other satellite-based experiments such as HEAO-1 [69], INTEGRAL [70], COMPTEL [76], EGRET [77] are sensitive to photons with energies well below a $\mathcal{O}(100)$ MeV. In this model, only HEAO-1 [69] and INTEGRAL [70] can put stringent constraints on the dark matter parameters as we are interested in the dark matter mass less than $\mathcal{O}(1)$ MeV. In Fig. 10, we show ² the limits coming from HEAO-1 [69] and INTEGRAL [70] in $y_{s\ell} - vs - M_{A_s^0}$ plane which puts a strong upper bound on the value of $y_{s\ell} \leq 10^{-6} - 10^{-7}$. However, as we are considering the non-thermal

² We extract these data from Ref. [73] where the authors have put bounds on the lifetime of a scalar dark matter decaying to two photons. We translate it into the interaction strength ($y_{s\ell}$), i.e. the interaction between dark matter, SM and mirror leptons, to constrain our model parameter space.

production of dark matter, the relic density can still be satisfied with smaller $y_{s\ell}$ as shown in the blue line in Fig. 10.

Now we turn our attention to the question of possible detection for this dark matter candidate A_s^0 at the current DM direct detection experiments. Motivated by the fact that the WIMP dark matter interacts with the matter weakly, there are many experiments [78–80] seeking to detect the dark matter directly. If the dark matter scatters from atomic nucleus depositing energy in the detector $E_{deposit} = \frac{m_r^2 v^2}{m_N} (1 - \cos \theta)$, where, m_r is the reduced mass of the dark matter $M_{A_s^0}$ and nucleons m_N , $v = 220 \text{ km/s}$ is the relative velocity of the dark matter w.r.t. detector nucleons and θ being the scattering angle, we find that for the tentative amount of deposited energy for a 100 GeV dark matter particle is 27 keV. It is to be noted that a cosmic radiation free and radioactively clean environment is needed for the detection of dark matter in these experiments with the set up placed in the deep underground [78–81] to reduce these backgrounds. Now, the DM direct detection experiments involve the CP-even Higgs-mediated t -channel process $A_s^0 N \rightarrow A_s^0 N$ (N is the nucleons) with a cross-section proportional to square of the quartic coupling $\lambda's = \lambda_{4a}, \lambda_{5c}$ and λ_s . It also has extra suppression due to the heavy mediator CP-even Higgs particles. The cross-section is given by

$$\sigma_{A_s^0, N} \approx \frac{m_r^2}{\pi} f^2 m_N^2 \left(\sum_i \frac{\lambda's}{M_{A_s^0} M_{\tilde{H}_i}^2} \right)^2 \quad (7.1)$$

where $f \approx 0.3$ is the form factor of the nucleus. m_r represents the reduced mass of the nucleus and the scattered dark matter particle. It is to be noted that $\lambda_{4a,5c,s} < 10^{-10}$ is needed to get the relic density for $< 1 \text{ MeV}$ dark matter (already discussed in the section VI). The direct detection cross-section become $< \mathcal{O}(10^{-61}) \text{ cm}^2$, far below the neutrino background events in the detector. Similarly mirror fermions mediated t -channel process $A_s^0 N \rightarrow A_s^0 N$ with a cross-section proportional to $y_{s\ell, sq}^4 / M_{MF}^4$ and the direct detection cross-section through mirror fermions exchange is far smaller than the scalar mediated diagram. Hence it is hard to get the signature of the dark matter form the direct-detection experiments through nucleon-dark matter scattering [81].

We have also investigated the dark matter-electron interactions via magnon excitations, a novel detection path for spin-dependent light that has been proposed in the recent work [82]. Magnons are quanta of collective spin wave excitations in condensed matter systems that exhibit magnetic dipole order in the ground state. It can be used as the spin-dependent counterpart of phonons for

the DM detection with similar kinematics. In future this type of experimental model may detect the dark matter (in particular pseudo scalar dark matter candidates) using absorption through magnon excitations or will be able to put stringent constraints on the parameter spaces. However currently in the current framework, the cross-section remain $< \mathcal{O}(10^{-61}) \text{ cm}^2$ for $\lambda_{4a,5c,s} < 10^{-10}$. Hence this method is unable to put farther constraints on this model.

The interactions of the mirror fermions with standard model particles make them more feasible to probe via the Collider searches. The existing literature (see Ref. [83]) includes possible ways to explore dark matter. The Ref. [83] has primarily investigated the FIMP dark matter scenario in the context of 14 TeV LHC experiments with a future high integrated luminosity at the MATHUSLA surface detector. In this framework, there is a possibility of forming a charged track due to the mirror fermions decay into SM fermion and dark matter fields at the Colliders. The decay width of the charged mirror fermion is given in eqn. 6.16. The decay width ($\Gamma(f_{MF} \rightarrow f_{SM} A_s^0)$) for the mirror fermions is proportional to $y_{s\ell}^2$ and masses of the mirror fermions. As discussed previously, an estimated value of the coupling $y_{s\ell} \lesssim 10^{-8}$ is needed to obtain the correct dark matter density through the Freeze-in process. We find the decay length for these charged fermions to be $\mathcal{O}(1)$ meter for this choice of $y_{s\ell}$. We are interested to see if we can get sufficient number of events from this charged tracks for the detection. It mainly depends on the production cross-section $\sigma_{\sqrt{s}}^{\text{LHC}}$ of the mother particle and luminosity \mathcal{L} at the detector. The number of events at the LHC is calculated in Ref. [83] and is given by

$$N_{events} = \sigma_{\sqrt{s}}^{\text{LHC}} \mathcal{L} \int P_{\text{Decay}}^{\text{MATH}}, \quad \text{with} \quad P_{\text{Decay}}^{\text{MATH}} = 0.05(e^{-\frac{L_a}{\beta c \tau_{f_{MF}}}} - e^{-\frac{L_b}{\beta c \tau_{f_{MF}}}}). \quad (7.2)$$

It has been reported in Ref. [83] that the number of events is $N_{events} \geq 3$ for $\sqrt{s} = 13 \text{ TeV}$ with an integrated luminosity $\mathcal{L} = 3000 \text{ fb}^{-1}$ using a specific model parameter space, showing that the MATHUSLA100/200 detector could detect these mother particle up to 1 TeV mass and the dominant production of the mother particles comes through the Drell-Yan processes. Following this reference, in our model, as the production of the mother particles (mirror fermions) are hugely suppressed due to the small mixing (see the BPs) of the mirror and standard model particles, we find the production cross-section is less than $\mathcal{O}(10^{-10}) \text{ fb}$. Hence it might need larger luminosity and energy to get significant events at the present MATHUSLA surface detector for our analysis.

VIII. CONCLUSION

In this work, we have presented a model incorporating a sub-MeV DM based on the exploration of the scalar sector of the Electroweak-scale Right-handed neutrino model. The idea of $\text{EW-}\nu_R$ model with additional GeV scale mirror fermions with large displaced vertices containing long lived particles (LLP) signatures is already highly appealing from the LHC perspective and has been extensively studied before [48, 84, 85]. The rich scalar sector of $\text{EW-}\nu_R$ includes doublets, triplets and an additional complex-singlet scalar Φ_s and the imaginary part of this complex singlet (pseudo-Nambu Goldstone (PNG) boson), A_s^0 is investigated to be a plausible DM candidate in the present context. The dark matter A_s^0 acquires a sub-MeV mass from the explicit breaking term in the scalar potential; this explicit breaking term is characterized by some mass scale assumed to be much smaller than the scale of spontaneous symmetry breaking (SSB). The various model parameters present in the scalar sector of this framework are investigated to generate possible benchmark points in the context of a sub-MeV dark matter, satisfying the current 125 GeV Higgs branching ratio and signal strength constraints from the LHC. In this work, we have shown the limitations of the well established Freeze out mechanism, for which the observed abundance is set almost exclusively by the annihilation cross-section and is largely insensitive to unknown details of early Universe and to the mass, producing overabundance for the sub-MeV DM particle A_s^0 we are interested to study in this work. Null results at direct detection experiments have currently put tight constraints on the WIMP paradigm and alternative possibilities like ALP, axions, SIMPs, FIMPS have become relevant in this context. We have implemented the Freeze-in mechanism to obtain the correct order of relic density for the chosen dark matter masses < 1 MeV. For such feebly interacting massive particles or FIMPs, we can invoke the non-thermal Freeze-in mechanism that necessitates feeble interactions making it one of the reasons to have such a tiny fine-tuned coupling present in this $\text{EW-}\nu_R$ model. We find that the non-thermally produced PSS (pseudo-scalar singlet) can serve as a viable ≤ 1 MeV dark matter depending on the parameters $\lambda_{5c}, \lambda_{4a}, \lambda_s, y_s, y_{s\ell}$ and VEVs satisfying the dark matter relic density.

Using the Freeze in mechanism to investigate the scalar sector of the $\text{EW-}\nu_R$, we obtain a significant parameter space of $y_{s\ell} - M_{A_s^0}$ for the sub-MeV dark matter mass satisfying the correct relic density and successfully put bounds on the coupling strength $y_{s\ell}$ vs $M_{A_s^0}$ exclusion region from the stability

(lifetime of DM > lifetime of the Universe) of the dark matter, the rare processes ($\mu \rightarrow e\gamma$, and $\mu - e$ conversion), several indirect detection experiments constraining this particular mass region (HEAO-1 and INTEGRAL) etc. We also found that indirect detection experiments, such as Fermi-LAT data are currently unable to successfully constrain the parameter space of $y_{s\ell} - M_{A_s^0}$ for the mass range of < 1 MeV. Also, due to such feeble interactions, it is challenging to get handle on the signatures of this light dark matter from the direct-detection experiments through nucleon-dark matter scattering as well as dark matter-electron interactions via the magnon excitations.

In our investigation, we have found that $y_{s\ell} \sim 10^{-8}$ is needed for the correct relic abundance and have pointed out the parameter space available for sub-MeV FIMP dark matter ready to be explored by the future experiments. We have discussed in detail the possible future implications of this scenario in the Collider searches, in specific the MATHUSLA detector. From a particle physics point of view, this scenario is highly interesting as the model framework has already been successful incorporating the non sterile right handed neutrinos with Electroweak scale Majorana masses. Having a substantial parameter space available to explore after implementing relevant constraints for a natural sub-MeV FIMP Dark matter particle in the current and future experiments makes this scenario even more relevant and exciting. The current framework casts light on the feebly explored sub-MeV dark sector frontier, and offers many opportunities for exciting and profound discoveries in the future.

IX. ACKNOWLEDGEMENTS

SC is supported by the College of Holy Cross Bachelor Ford Summer fellowship '20-'21. DKG, NK and DN would like to thank Prof. Satyanarayan Mukhopadhyay and Dr. Anirban Biswas for useful discussions.

Appendix A: Model: Scalar sector

The model framework and motivations including the gauge structure, particle content [30] has already been introduced previously in this work. Here we include a summary of the details on the extended scalar sector of the Electro-weak Right handed neutrino model that is vital for studying

the dark matter portion of this framework. The present framework includes a rich scalar sector incorporating four doublets (two for the THDM like, two for mirror sector), two triplets and a singlet given by

$$\Phi_1 = \begin{pmatrix} \phi_1^{0,*} & \phi_1^+ \\ \phi_1^- & \phi_1^0 \end{pmatrix}, \quad \Phi_{1M} = \begin{pmatrix} \phi_{1M}^{0,*} & \phi_{1M}^+ \\ \phi_{1M}^- & \phi_{1M}^0 \end{pmatrix}, \quad \Phi_2 = \begin{pmatrix} \phi_2^{0,*} & \phi_2^+ \\ \phi_2^- & \phi_2^0 \end{pmatrix}, \quad \Phi_{2M} = \begin{pmatrix} \phi_{2M}^{0,*} & \phi_{2M}^+ \\ \phi_{2M}^- & \phi_{2M}^0 \end{pmatrix},$$

$$\tilde{\chi} = \begin{pmatrix} \chi^+/\sqrt{2} & \chi^{++} \\ \chi^0 & -\chi^+/\sqrt{2} \end{pmatrix}, \quad \xi = (\xi^+, \xi^0, \xi^-), \quad \text{Complex singlet scalar} = \Phi_s \quad (\text{A1})$$

The transformation of these scalar multiplet under $U(1)_{\text{SM}} \times U(1)_{\text{MF}}$ symmetry are as follows: $\Phi_{1,2} \rightarrow e^{-2i\alpha_{\text{SM}}} \Phi_{1,2}$, $\Phi_{1M,2M} \rightarrow e^{2i\alpha_{\text{MF}}} \Phi_{1M,2M}$, $\tilde{\chi} \rightarrow e^{-2i\alpha_{\text{MF}}} \tilde{\chi}$, $\xi \rightarrow \xi$ and $\Phi_s \rightarrow e^{-i(\alpha_{\text{SM}} + \alpha_{\text{MF}})} \Phi_s$. Additionally, the Higgs potential has a global $SU(2)_L \times SU(2)_R$ symmetry. The triplet and doublet scalars transform as $(3, 3)$ and $(2, 2)$ under that global symmetry. The combination of these triplet can be written as [30]

$$\chi = \begin{pmatrix} \chi^0 & \xi^+ & \chi^{++} \\ \chi^- & \xi^0 & \chi^+ \\ \chi^{--} & \xi^- & \chi^{0,*} \end{pmatrix}, \quad (\text{A2})$$

Proper vacuum alignment gives

$$\langle \Phi_1 \rangle = \begin{pmatrix} v_1/\sqrt{2} & 0 \\ 0 & v_1/\sqrt{2} \end{pmatrix}, \quad \langle \Phi_{1M} \rangle = \begin{pmatrix} v_{1M}/\sqrt{2} & 0 \\ 0 & v_{1M}/\sqrt{2} \end{pmatrix}, \quad (\text{A3})$$

$$\langle \Phi_2 \rangle = \begin{pmatrix} v_2/\sqrt{2} & 0 \\ 0 & v_2/\sqrt{2} \end{pmatrix}, \quad \langle \Phi_{2M} \rangle = \begin{pmatrix} v_{2M}/\sqrt{2} & 0 \\ 0 & v_{2M}/\sqrt{2} \end{pmatrix}, \quad (\text{A4})$$

$$\langle \chi \rangle = \begin{pmatrix} v_M & 0 & 0 \\ 0 & v_M & 0 \\ 0 & 0 & v_M \end{pmatrix}, \quad \langle \Phi_s \rangle = v_s \quad (\text{A5})$$

The generic scalar potential for these scalars can now be written as

$$V = \lambda_{1a} \left[\text{Tr} \Phi_1^\dagger \Phi_1 - v_1^2 \right]^2 + \lambda_{2a} \left[\text{Tr} \Phi_{1M}^\dagger \Phi_{1M} - v_{1M}^2 \right]^2 + \lambda_{1b} \left[\text{Tr} \Phi_2^\dagger \Phi_2 - v_2^2 \right]^2 + \lambda_{2b} \left[\text{Tr} \Phi_{2M}^\dagger \Phi_{2M} - v_{2M}^2 \right]^2 + \lambda_3 \left[\text{Tr} \chi^\dagger \chi - 3v_M^2 \right]^2$$

$$\begin{aligned}
& + \lambda_s \left[\Phi_s^\dagger \Phi_s - v_s^2 \right]^2 + \lambda_4 \left[Tr \Phi_1^\dagger \Phi_1 - v_1^2 + Tr \Phi_{1M}^\dagger \Phi_{1M} - v_{1M}^2 \right. \\
& \quad \left. + Tr \Phi_2^\dagger \Phi_2 - v_2^2 + Tr \Phi_{2M}^\dagger \Phi_{2M} - v_{2M}^2 + Tr \chi^\dagger \chi - 3v_M^2 \right]^2 \\
& + \lambda_{4a} \left[Tr \Phi_1^\dagger \Phi_1 - v_1^2 + Tr \Phi_{1M}^\dagger \Phi_{1M} - v_{1M}^2 + Tr \Phi_2^\dagger \Phi_2 - v_2^2 \right. \\
& \quad \left. + Tr \Phi_{2M}^\dagger \Phi_{2M} - v_{2M}^2 + Tr \chi^\dagger \chi - 3v_M^2 \right] \left[\Phi_s^\dagger \Phi_s - v_s^2 \right] \\
& + \lambda_{5a} \left[(Tr \Phi_1^\dagger \Phi_1) (Tr \chi^\dagger \chi) - 2(Tr \Phi_1^\dagger \frac{\tau^a}{2} \Phi_1 \frac{\tau^b}{2}) (Tr \chi^\dagger T^a \chi T^b) \right] \\
& + \lambda_{6a} \left[(Tr \Phi_{1M}^\dagger \Phi_{1M}) (Tr \chi^\dagger \chi) - 2(Tr \Phi_{1M}^\dagger \frac{\tau^a}{2} \Phi_{1M} \frac{\tau^b}{2}) (Tr \chi^\dagger T^a \chi T^b) \right] \\
& + \lambda_{5b} \left[(Tr \Phi_2^\dagger \Phi_2) (Tr \chi^\dagger \chi) - 2(Tr \Phi_2^\dagger \frac{\tau^a}{2} \Phi_2 \frac{\tau^b}{2}) (Tr \chi^\dagger T^a \chi T^b) \right] \\
& + \lambda_{6b} \left[(Tr \Phi_{2M}^\dagger \Phi_{2M}) (Tr \chi^\dagger \chi) - 2(Tr \Phi_{2M}^\dagger \frac{\tau^a}{2} \Phi_{2M} \frac{\tau^b}{2}) (Tr \chi^\dagger T^a \chi T^b) \right] \\
& + \lambda_{5c} \left[\{ \Phi_s^2 (Tr \Phi_1^\dagger \Phi_{1M} + Tr \Phi_1^\dagger \Phi_{2M} + Tr \Phi_2^\dagger \Phi_{1M} + Tr \Phi_2^\dagger \Phi_{2M}) + h.c. \} \right. \\
& \quad \left. - 2 \Phi_s^\dagger \Phi_s (Tr \Phi_1^\dagger \Phi_{1M} + Tr \Phi_1^\dagger \Phi_{2M} + Tr \Phi_2^\dagger \Phi_{1M} + Tr \Phi_2^\dagger \Phi_{2M}) \right] \\
& + \lambda_{7a} \left[(Tr \Phi_1^\dagger \Phi_1) (Tr \Phi_{1M}^\dagger \Phi_{1M}) - (Tr \Phi_1^\dagger \Phi_{1M}) (Tr \Phi_{1M}^\dagger \Phi_1) \right] \\
& + \lambda_{7b} \left[(Tr \Phi_2^\dagger \Phi_2) (Tr \Phi_{2M}^\dagger \Phi_{2M}) - (Tr \Phi_2^\dagger \Phi_{2M}) (Tr \Phi_{2M}^\dagger \Phi_2) \right] \\
& + \lambda_{7ab} \left[(Tr \Phi_1^\dagger \Phi_1) (Tr \Phi_2^\dagger \Phi_2) - (Tr \Phi_1^\dagger \Phi_2) (Tr \Phi_2^\dagger \Phi_1) \right] \\
& + \lambda_{7Mab} \left[(Tr \Phi_{1M}^\dagger \Phi_{1M}) (Tr \Phi_{2M}^\dagger \Phi_{2M}) - (Tr \Phi_{1M}^\dagger \Phi_{2M}) (Tr \Phi_{2M}^\dagger \Phi_{1M}) \right] \\
& + \lambda_{7aMb} \left[(Tr \Phi_1^\dagger \Phi_1) (Tr \Phi_{2M}^\dagger \Phi_{2M}) - (Tr \Phi_1^\dagger \Phi_{2M}) (Tr \Phi_{2M}^\dagger \Phi_1) \right] \\
& + \lambda_{7abM} \left[(Tr \Phi_2^\dagger \Phi_2) (Tr \Phi_{1M}^\dagger \Phi_{1M}) - (Tr \Phi_2^\dagger \Phi_{1M}) (Tr \Phi_{1M}^\dagger \Phi_2) \right] \\
& + \lambda_8 \left[Tr \chi^\dagger \chi \chi^\dagger \chi - (Tr \chi^\dagger \chi)^2 \right], \tag{A6}
\end{aligned}$$

where $a, b = 1, 2, 3$ and from [86]

$$T^1 = \frac{1}{\sqrt{2}} \begin{pmatrix} 0 & 1 & 0 \\ 1 & 0 & 1 \\ 0 & 1 & 0 \end{pmatrix}; \quad T^2 = \frac{1}{\sqrt{2}} \begin{pmatrix} 0 & -i & 0 \\ i & 0 & -i \\ 0 & i & 0 \end{pmatrix}; \quad T^3 = \begin{pmatrix} 1 & 0 & 0 \\ 0 & 0 & 0 \\ 0 & 0 & -1 \end{pmatrix}; \tag{A7}$$

$$\tau^1 = \begin{pmatrix} 0 & 1 \\ 1 & 0 \end{pmatrix}; \quad \tau^2 = \begin{pmatrix} 0 & -i \\ i & 0 \end{pmatrix}; \quad \tau^3 = \begin{pmatrix} 1 & 0 \\ 0 & -1 \end{pmatrix}; \tag{A8}$$

Please note the transformation $\Phi_{1,2} \rightarrow e^{-2i\alpha_{\text{SM}}} \Phi_{1,2}$, $\Phi_{1M,2M} \rightarrow e^{2i\alpha_{\text{MF}}} \Phi_{1M,2M}$, $\tilde{\chi} \rightarrow e^{-2i\alpha_{\text{MF}}} \tilde{\chi}$, $\xi \rightarrow \xi$ and $\Phi_s \rightarrow e^{-i(\alpha_{\text{SM}} + \alpha_{\text{MF}})} \Phi_s$. Hence the $\lambda_{5,6}$'s terms break explicitly the $U(1)_{\text{SM}} \times U(1)_{\text{MF}}$ symmetries. The three ‘massless’ Nambu-Goldstone bosons can be obtained after spontaneous breaking of $SU(2)_L \times U(1)_Y \rightarrow U(1)_{\text{em}}$, with the condition $\lambda_{5a} = \lambda_{5b} = \lambda_{6a} = \lambda_{6b} = \lambda_{7a} = \lambda_{7b} = \lambda_{7ab} = \lambda_{7aM} = \lambda_{7abM} = \lambda_5$ imposed on the potential above. The first line of λ_{5c} term is $U(1)_{\text{SM}} \times U(1)_{\text{MF}}$ conserving, and the second line explicitly violates these symmetries. Both of them will help us to get exact minimization of the scalar potential and non-zero mass for the singlet-type complex scalar field. There are eighteen physical scalars grouped into $5 + 3 + 3 + 3 + 3 + 1$ of the custodial $SU(2)_D$ with 6 real singlets. Here, we would like to mention that the dedicated study of vacuum stability condition for a multi-Higgs model like ours is extremely complicated and is beyond the scope of this paper.

To express the Nambu-Goldstone bosons and the physical scalars let us adopt the following convenient notation:

$$\begin{aligned}
v_{\text{SM}} &= \sqrt{v_1^2 + v_{1M}^2 + v_2^2 + v_{2M}^2 + 8v_M^2} \approx 246 \text{ GeV} \\
s_1 &= \frac{v_1}{v_{\text{SM}}}, \quad c_1 = \frac{\sqrt{v_{1M}^2 + v_2^2 + v_{2M}^2 + 8v_M^2}}{v_{\text{SM}}}, \\
s_2 &= \frac{v_2}{v_{\text{SM}}}, \quad c_2 = \frac{\sqrt{v_{1M}^2 + v_1^2 + v_{2M}^2 + 8v_M^2}}{v_{\text{SM}}}, \\
s_{1m} &= \frac{v_{1M}}{v_{\text{SM}}}, \quad c_{1m} = \frac{\sqrt{v_1^2 + v_2^2 + v_{2M}^2 + 8v_M^2}}{v_{\text{SM}}}, \\
s_{2m} &= \frac{v_{2M}}{v_{\text{SM}}}, \quad c_{2m} = \frac{\sqrt{v_1^2 + v_{1M}^2 + v_2^2 + 8v_M^2}}{v_{\text{SM}}}, \\
s_m &= \frac{2\sqrt{2}v_M}{v_{\text{SM}}}, \quad c_m = \frac{\sqrt{v_1^2 + v_{1M}^2 + v_2^2 + v_{2M}^2}}{v_{\text{SM}}}.
\end{aligned} \tag{A9}$$

Thus, $s_1^2 + c_1^2 = s_2^2 + c_2^2 = s_{1m}^2 + c_{1m}^2 = s_{2m}^2 + c_{2m}^2 = s_m^2 + c_m^2 = 1$. We also defined

$$\begin{aligned}
\phi_1^0 &= \frac{1}{\sqrt{2}}(\phi_1^{0r} + v_1 + i\phi_1^{0i}), \quad \phi_2^0 = \frac{1}{\sqrt{2}}(\phi_2^{0r} + v_2 + i\phi_2^{0i}), \\
\phi_{1M}^0 &= \frac{1}{\sqrt{2}}(\phi_{1M}^{0r} + v_{1M} + i\phi_{1M}^{0i}), \quad \phi_{2M}^0 = \frac{1}{\sqrt{2}}(\phi_{2M}^{0r} + v_{2M} + i\phi_{2M}^{0i}), \\
\chi^0 &= \frac{1}{\sqrt{2}}(\chi^{0r} + v_M + i\chi^{0i}), \quad \xi^0 = (\xi^0 + v_M), \quad \Phi_s = \phi_s^{0r} + v_s + i\phi_s^{0i} \\
\text{and } \psi^\pm &= \frac{1}{\sqrt{2}}(\chi^\pm + \xi^\pm), \quad \zeta^\pm = \frac{1}{\sqrt{2}}(\chi^\pm - \xi^\pm).
\end{aligned}$$

for the complex neutral and charged fields respectively. With these fields the Nambu-Goldstone bosons are given by

$$\begin{aligned} y_1^\pm &= s_1\phi_1^\pm + s_2\phi_2^\pm + s_{1M}\phi_{1M}^\pm + s_{2M}\phi_{2M}^\pm + s_M\psi^\pm, \\ y_1^0 &= -i(s_1\phi_1^{0i} + s_2\phi_2^{0i} + s_{1M}\phi_{1M}^{0i} + s_{2M}\phi_{2M}^{0i}) + is_M\chi^{0i}. \end{aligned} \quad (\text{A10})$$

The physical scalars can be grouped, as stated in the previous section, based on their transformation properties under $SU(2)_D$ as follows:

$$\begin{aligned} \text{five-plet (quintet)} &\rightarrow H_5^{\pm\pm}, H_5^\pm, \text{ and } H_5^0 \\ \text{triplet} &\rightarrow H_3^\pm, \text{ and } H_3^0 \\ \text{triplet} &\rightarrow H_3'^\pm, \text{ and } H_3'^0 \\ \text{triplet} &\rightarrow H_M^\pm, \text{ and } H_M^0 \\ \text{triplet} &\rightarrow H_M'^\pm, \text{ and } H_M'^0 \end{aligned} \quad (\text{A11})$$

$$\begin{aligned} \text{Real singlet} &\rightarrow H_1^0, H_2^0, H_{1M}^0, H_{2M}^0, H_1^{0'}, \text{ and } H_s^0 \end{aligned} \quad (\text{A12})$$

where,

$$\begin{aligned} H_5^{\pm\pm} &= \chi^{\pm\pm}, \quad H_5^\pm = \zeta^\pm, \quad H_5^0 = \frac{1}{\sqrt{6}}(2\zeta^0 - \sqrt{2}\chi^{0r}), \\ H_3^+ &= -\frac{s_1s_M}{c_M}\phi_1^+ - \frac{s_2s_M}{c_M}\phi_2^+ - \frac{s_{1M}s_M}{c_M}\phi_{1M}^+ - \frac{s_{2M}s_M}{c_M}\phi_{2M}^+ + c_M\psi_M \\ H_3^0 &= i\left(\frac{s_1s_M}{c_M}\phi_1^{0i} + \frac{s_2s_M}{c_M}\phi_2^{0i} + \frac{s_{1M}s_M}{c_M}\phi_{1M}^{0i} + \frac{s_{2M}s_M}{c_M}\phi_{2M}^{0i} + c_M\chi^{0i}\right) \\ H_3'^+ &= \frac{s_1}{c_M}\phi_2^+ - \frac{s_2}{c_M}\phi_1^+ + \frac{s_{1M}}{c_M}\phi_{2M}^+ - \frac{s_{2M}}{c_M}\phi_{1M}^+ \\ H_3'^0 &= i\left(\frac{s_1}{c_M}\phi_2^{0i} - \frac{s_2}{c_M}\phi_1^{0i} + \frac{s_{1M}}{c_M}\phi_{2M}^{0i} - \frac{s_{2M}}{c_M}\phi_{1M}^{0i}\right) \end{aligned} \quad (\text{A13})$$

$$\begin{aligned} H_{3M}^+ &= \frac{s_{1M}}{c_M}\phi_2^+ - \frac{s_{2M}}{c_M}\phi_1^+ + \frac{s_1}{c_M}\phi_{2M}^+ - \frac{s_2}{c_M}\phi_{1M}^+ \\ H_{3M}^0 &= i\left(\frac{s_{1M}}{c_M}\phi_2^{0i} - \frac{s_{2M}}{c_M}\phi_1^{0i} + \frac{s_1}{c_M}\phi_{2M}^{0i} - \frac{s_2}{c_M}\phi_{1M}^{0i}\right) \end{aligned}$$

$$\begin{aligned}
H'_{M3}^+ &= \frac{s_{2M}}{c_M} \phi_2^+ - \frac{s_{1M}}{c_M} \phi_1^+ - \frac{s_2}{c_M} \phi_{2M}^+ + \frac{s_1}{c_M} \phi_{1M}^+ \\
H'^0_{M3} &= i \left(\frac{s_{2M}}{c_M} \phi_2^{0i} - \frac{s_{1M}}{c_M} \phi_1^{0i} - \frac{s_2}{c_M} \phi_2^{0i} + \frac{s_1}{c_M} \phi_{1M}^{0i} \right)
\end{aligned}$$

$$\begin{aligned}
H_1^0 &= \phi_1^{0r}, \quad H_2^0 = \phi_2^{0r}, \quad H_{1M}^0 = \phi_{1M}^{0r}, \quad H_{2M}^0 = \phi_{2M}^{0r}, \\
H_s^0 &= \phi_s^{0r}, \quad \text{and} \quad H_1^{0'} = \sqrt{\frac{2}{3}} \chi^{0r} + \sqrt{\frac{1}{3}} \zeta^0,
\end{aligned}$$

where, $H^{--} = (H^{++})^*$, $H_{\text{All}}^- = -(H_{\text{All}}^+)^*$, $H_{\text{All}}^0 = -(H_{\text{All}}^0)^*$. The masses of these physical scalars can easily be obtained from Eq. eq:pot. Since, the potential preserves the $SU(2)_D$ custodial symmetry, members of the physical scalar multiplets have degenerate masses. These masses are

$$\begin{aligned}
m_5^2 &= 3 (\lambda_5 (v_1^2 + v_{1M}^2 + v_2^2 + v_{2M}^2) + 8\lambda_8 v_{3M}^2) \equiv 3 (\lambda_5 c_m^2 + 8\lambda_8 s_m^2) v_{\text{SM}}^2, \\
m_{3,H^\pm,H_3^0}^2 &= \lambda_5 (v_1^2 + v_{1M}^2 + v_2^2 + v_{2M}^2 + 8v_{3M}^2) \equiv \lambda_5 v_{\text{SM}}^2 \\
m_{3,\text{All others}}^2 &= 2\lambda_5 (v_1^2 + v_{1M}^2 + v_2^2 + v_{2M}^2 + 4v_{3M}^2) \equiv \lambda_5 (1 + c_m^2) v_{\text{SM}}^2. \tag{A14}
\end{aligned}$$

In general, H_1^0 , H_2^0 , H_{1M}^0 , H_{2M}^0 , H_s^0 and $H_1^{0'}$ can mix according to the mass-squared matrix

$$\mathcal{M}_{\mathcal{H}}^2 = v_{\text{SM}}^2 \begin{pmatrix} 8(\lambda_{1a} + \lambda_4)s_1^2 & 8\lambda_4 s_1 s_2 & 8\lambda_4 s_1 s_m & 8\lambda_4 s_1 s_{2m} & 8\lambda_4 a \frac{v_s s_1}{v_{\text{SM}}} & 2\sqrt{6}\lambda_4 s_1 s_m \\ 8\lambda_4 s_1 s_2 & 8(\lambda_{1b} + \lambda_4)s_2^2 & 8\lambda_4 s_2 s_m & 8\lambda_4 s_2 s_{2m} & 8\lambda_4 a \frac{v_s s_2}{v_{\text{SM}}} & 2\sqrt{6}\lambda_4 s_2 s_m \\ 8\lambda_4 s_1 s_m & 8\lambda_4 s_2 s_m & 8(\lambda_{2a} + \lambda_4)s_m^2 & 8\lambda_4 s_m s_{2m} & 8\lambda_4 a \frac{v_s s_m}{v_{\text{SM}}} & 2\sqrt{6}\lambda_4 s_m^2 \\ 8\lambda_4 s_1 s_{2m} & 8\lambda_4 s_2 s_{2m} & 8\lambda_4 s_m s_{2m} & 8(\lambda_{2b} + \lambda_4)s_{2m}^2 & 8\lambda_4 a \frac{v_s s_{2m}}{v_{\text{SM}}} & 2\sqrt{6}\lambda_4 s_m s_{2m} \\ 8\lambda_4 a \frac{v_s s_1}{v_{\text{SM}}} & 8\lambda_4 a \frac{v_s s_2}{v_{\text{SM}}} & 8\lambda_4 a \frac{v_s s_m}{v_{\text{SM}}} & 8\lambda_4 a \frac{v_s s_{2m}}{v_{\text{SM}}} & 8(\lambda_{4a} + \lambda_s) \frac{v_s^2}{v_{\text{SM}}^2} & 2\sqrt{6}\lambda_4 a \frac{v_s s_m}{v_{\text{SM}}} \\ 2\sqrt{6}\lambda_4 s_1 s_m & 2\sqrt{6}\lambda_4 s_2 s_m & 2\sqrt{6}\lambda_4 s_m^2 & 2\sqrt{6}\lambda_4 s_m s_{2m} & 2\sqrt{6}\lambda_4 a \frac{v_s s_m}{v_{\text{SM}}} & 3(\lambda_3 + \lambda_4)s_m^2 \end{pmatrix} \tag{A15}$$

We denote the mass eigenstates by \tilde{H}'''' , \tilde{H}''' , \tilde{H}'' , \tilde{H}' , \tilde{H} , \tilde{H}_s . We adopt a convention of denoting the lightest of the six by \tilde{H}_s . The next heavier one by \tilde{H} , the next one is \tilde{H}' and so on. The heaviest state is \tilde{H}'''' . The descending order of mass of the physical eigenstates is $(M_{\tilde{H}''''} > M_{\tilde{H}'''}) > M_{\tilde{H}''} > M_{\tilde{H}'} > M_{\tilde{H}} > M_{\tilde{H}_s})$. The diagonalizing 6×6 orthogonal matrix element is denoted by O_H^{ij} ($i, j = 1 \dots 6$). The 125-GeV Higgs-like scalar component can be written as

$$\tilde{H} = O_H^{51} H_1^0 + O_H^{52} H_2^0 + O_H^{53} H_{1M}^0 + O_H^{54} H_{2M}^0 + O_H^{55} H_s^0 + O_H^{56} H_1^{0'} \tag{A16}$$

The SM fermion sector in this EW- ν_R model are given by [27, 37, 41, 48]

$$\psi_L = \begin{pmatrix} \nu_\ell \\ \ell \end{pmatrix}_L, \quad \text{and} \quad \ell_R, \quad Q_L = \begin{pmatrix} u \\ d \end{pmatrix}_L, \quad u_R \quad \text{and} \quad d_R, \quad (\text{A17})$$

where $\ell = e, \mu, \tau$ and u stands for the *up-type* quarks (u, c, t) and d denotes the *down-type* quarks (d, s, b). L indicates the left-chirality and R is right-chirality. In the EW- ν_R model, right-handed neutrinos are parts of $SU(2)$ doublets along with their charged partners (the mirror charged leptons). Anomaly freedom dictates the existence of doublets of right-handed and singlets left-handed mirror quarks [27, 37, 41, 48]

$$\psi_R^M = \begin{pmatrix} \nu_\ell^M \\ \ell^M \end{pmatrix}_R, \quad \text{and} \quad \ell_L^M, \quad Q_R^M = \begin{pmatrix} u^M \\ d^M \end{pmatrix}_R, \quad u_L^M \quad \text{and} \quad d_L^M \quad (\text{A18})$$

It is noted that all other fields ($SU(2)$ -singlet right-handed SM fermions, left-handed mirror fermions) are taken to be singlet under $U(1)_{\text{SM}} \times U(1)_{\text{MF}}$ transformation in Ref. [27, 48]. To solve the strong CP problem, we follow different transformation as in Ref. [41]. The SM $SU(2)$ singlet fermions transform as $(\ell_R, u_R, d_R) \rightarrow e^{i\alpha_{\text{SM}}} (\ell_R, u_R, d_R)$ whereas $SU(2)$ singlet fermions go as $(\ell_R^M, u_R^M, d_R^M) \rightarrow e^{i\alpha_{\text{MF}}} (\ell_R^M, u_R^M, d_R^M)$.

The Higgs doublet Φ_2 only couples to SM *up-quarks* while another doublet Φ_1 couples to *down-quarks* and *leptons*. It behaves like type-II two Higgs doublet model. Similar interactions are also there in the mirror sector with Φ_{1M} and Φ_{2M} scalar doublets. The $\tilde{\chi}$ in the Higgs triplet fields with hypercharge $Y = 2$ and χ is a real Higgs triplet with $Y = 0$. S is a complex singlet scalar which helps to generate the neutrino observables and strong CP problems. The total Yukawa part of the Lagrangian is given by [27, 37, 41, 48]

$$\begin{aligned} \mathcal{L}_y = & y_\ell \bar{\psi}_L \Phi_1 \ell_R + y_\ell^M \bar{\psi}_R^M \Phi_{1M} \ell_R^M + y_{s\ell} \bar{\psi}_L \psi_R^M \Phi_s + y_M \psi_R^{M,T} iC\sigma_2 \tilde{\chi} \psi_R^M \\ & + y_d \bar{Q}_L \Phi_1 d_R + y_d^M \bar{Q}_R^M \Phi_{1M} d_R^M - y_u \bar{Q}_L i\sigma_2 \Phi_2 u_R - y_u^M \bar{Q}_R^M i\sigma_2 \Phi_{2M} u_R^M \\ & + y_{sd} \bar{d}_R d_L^M \Phi_s + y_{sq} \bar{Q}_L Q_R^M \Phi_s + y_{su} \bar{u}_R u_R^M \Phi_s + \text{h.c} \end{aligned} \quad (\text{A19})$$

where C is the charge conjugation operator, σ_2 being the second Pauli's spin matrix.

Now we will calculate the various mass-mixing matrix after electroweak symmetry breaking, physical mass eigenstates of the fermions in this model. The charged-lepton mixing matrix can be

found as [27]

$$\mathcal{M}_l = \begin{pmatrix} m_l & m_\nu^D \\ m_\nu^D & m_l^M \end{pmatrix}, \quad (\text{A20})$$

where, $m_\ell = y_\ell v_1/\sqrt{2}$, $m_\ell^M = y_\ell^M v_{1M}/\sqrt{2}$ and $m_\nu^D = y_{s\ell} v_s$. The l and ℓ^M stand for flavour eigenstates whereas $\tilde{\ell}$ and $\tilde{\ell}^M$ stand for the mass eigenstates. The mixing angle between ℓ and ℓ^M is θ_ℓ , hence $\tan 2\theta_\ell = \frac{2m_\nu^D}{m_\ell^M - m_\ell}$. The mixing matrix is $R_\ell = \{\{\cos \theta_\ell, \sin \theta_\ell\}, \{-\sin \theta_\ell, \cos \theta_\ell\}\}$. For $m_\ell^M \gg m_\ell, m_\nu^D$, one can write $\tan \theta_\ell \approx \sin \theta_\ell \approx \theta_\ell \approx \frac{m_\nu^D}{m_\ell^M} = \frac{\sqrt{2}y_{s\ell}v_s}{y_\ell^M v_{1M}}$. The mass eigenstates can be written as

$$\begin{aligned} \tilde{\ell} &= \ell \cos \theta_\ell + \ell^M \sin \theta_\ell \\ \tilde{\ell}^M &= -\ell \sin \theta_\ell + \ell^M \cos \theta_\ell \end{aligned} \quad (\text{A21})$$

As there is no singlet right-handed neutrino in this model, there is no such mixing in the neutrino sector and hence the pseudoscalar A_s^0 could not decay into two light neutrinos. The up and down sector mixing matrix are given by [40, 41]

$$\mathcal{M}_u = \begin{pmatrix} m_u & m_{sq} \\ m_{su} & m_u^M \end{pmatrix}, \quad \text{and} \quad \mathcal{M}_d = \begin{pmatrix} m_d & m_{sq} \\ m_{sd} & m_d^M \end{pmatrix}, \quad (\text{A22})$$

where, $m_d = y_d v_1/\sqrt{2}$, $m_d^M = y_d^M v_{1M}/\sqrt{2}$, $m_u = y_d v_2/\sqrt{2}$, $m_u^M = y_u^M v_{2M}/\sqrt{2}$, $m_{sq} \approx y_{sq} v_s$, $m_{su} \approx y_{su} v_s$ and $m_{su} \approx y_{sd} v_s$. The mixing matrix are $R_{u,d} = \{\{\cos \theta_{u,d}, \sin \theta_{u,d}\}, \{-\sin \theta_{u,d}, \cos \theta_{u,d}\}\}$, where

$$\sin \theta_u = \sqrt{\frac{(m_u^M - m_u) \left(m_u^M - m_u - \sqrt{(m_u^M - m_u)^2 + 4m_{sq}m_{su}} \right) + 2m_{sq}m_{su} + 2m_{su}^2}{2 \left((m_u^M - m_u)^2 + 2m_{sq}m_{su} + m_{sq}^2 + m_{su}^2 \right)}} \quad (\text{A23})$$

We can also get the similar analytical form of $\sin \theta_d$ by replacing u to d in eqn. A23. Let u, d and u^M, d^M stand for flavour eigenstates and \tilde{u}, \tilde{d} and \tilde{u}^M, \tilde{d}^M stand for the mass eigenstates. Thus one can write

$$\begin{aligned} \tilde{u} &= u \cos \theta_u + u^M \sin \theta_u \\ \tilde{u}^M &= -u \sin \theta_u + u^M \cos \theta_u \\ \tilde{d} &= d \cos \theta_d + d^M \sin \theta_d \end{aligned} \quad (\text{A24})$$

$$\tilde{d}^M = -d \sin \theta_d + d^M \cos \theta_d \quad (\text{A25})$$

The terms $(y_{s\ell} \bar{\psi}_L \psi_R^M + y_{sd} \bar{d}_R d_L^M + y_{sq} \bar{Q}_L Q_R^M + y_{su} \bar{u}_R u_L^M) \Phi_s$ in eqn A19 can help us to get the $A_s^0 \tilde{f}_i \tilde{f}_i$ coupling strengths. A_s^0 to two leptons (both the SM and MF charged and neutral leptons) can be written as

$$y_f^\ell = y_{s\ell} \sin \theta_\ell \cos \theta_\ell \gamma_5 \approx y_{s\ell} \sin \theta_\ell \gamma_5 \approx \sqrt{2} \frac{y_{s\ell}^2 v_s}{y_\ell^M v_{1M}} \gamma_5. \quad (\text{A26})$$

For $y_{sq} \sim y_{su} \sim y_{sd} = y_s$, $v_{1M} = v_{2M}$ and $y_d^M = y_u^M$, we can write the mixing angle $\theta_u = \theta_d \approx \frac{\sqrt{2} y_s v_s}{y_u^M v_{1M}}$. Similarly A_s^0 to two quarks (both the SM and MF up and down quarks) coupling strengths are given by

$$y_f^q = y_s \sin \theta_u \cos \theta_u \gamma_5 \approx y_s \sin \theta_u \gamma_5 \approx \sqrt{2} \frac{y_s^2 v_s}{y_u^M v_{1M}} \gamma_5. \quad (\text{A27})$$

[1] F. Zwicky, “Die Rotverschiebung von extragalaktischen Nebeln,” *Helv. Phys. Acta* **6** (1933) 110–127.

[2] V. C. Rubin and W. K. Ford, Jr., “Rotation of the Andromeda Nebula from a Spectroscopic Survey of Emission Regions,” *Astrophys. J.* **159** (1970) 379–403.

[3] D. Clowe, M. Bradac, A. H. Gonzalez, M. Markevitch, S. W. Randall, C. Jones, and D. Zaritsky, “A direct empirical proof of the existence of dark matter,” *Astrophys. J. Lett.* **648** (2006) L109–L113, [arXiv:astro-ph/0608407](https://arxiv.org/abs/astro-ph/0608407).

[4] R. Massey, T. Kitching, and J. Richard, “The dark matter of gravitational lensing,” *Rept. Prog. Phys.* **73** (2010) 086901, [arXiv:1001.1739 \[astro-ph.CO\]](https://arxiv.org/abs/1001.1739).

[5] **Planck** Collaboration, N. Aghanim *et al.*, “Planck 2018 results. VI. Cosmological parameters,” *Astron. Astrophys.* **641** (2020) A6, [arXiv:1807.06209 \[astro-ph.CO\]](https://arxiv.org/abs/1807.06209).

[6] S. Giagu, “WIMP Dark Matter Searches With the ATLAS Detector at the LHC,” *Front. in Phys.* **7** (2019) 75.

[7] **ATLAS** Collaboration, M. Aaboud *et al.*, “Search for dark matter in events with a hadronically decaying vector boson and missing transverse momentum in pp collisions at $\sqrt{s} = 13$ TeV with the ATLAS detector,” *JHEP* **10** (2018) 180, [arXiv:1807.11471 \[hep-ex\]](https://arxiv.org/abs/1807.11471).

[8] **ATLAS** Collaboration, M. Aaboud *et al.*, “Search for dark matter and other new phenomena in

events with an energetic jet and large missing transverse momentum using the ATLAS detector,” *JHEP* **01** (2018) 126, [arXiv:1711.03301 \[hep-ex\]](https://arxiv.org/abs/1711.03301).

[9] **ATLAS** Collaboration, M. Aaboud *et al.*, “Search for dark matter at $\sqrt{s} = 13$ TeV in final states containing an energetic photon and large missing transverse momentum with the ATLAS detector,” *Eur. Phys. J. C* **77** no. 6, (2017) 393, [arXiv:1704.03848 \[hep-ex\]](https://arxiv.org/abs/1704.03848).

[10] **ATLAS** Collaboration, M. Aaboud *et al.*, “Search for an invisibly decaying Higgs boson or dark matter candidates produced in association with a Z boson in pp collisions at $\sqrt{s} = 13$ TeV with the ATLAS detector,” *Phys. Lett. B* **776** (2018) 318–337, [arXiv:1708.09624 \[hep-ex\]](https://arxiv.org/abs/1708.09624).

[11] **LUX** Collaboration, D. S. Akerib *et al.*, “Results from a search for dark matter in the complete LUX exposure,” *Phys. Rev. Lett.* **118** no. 2, (2017) 021303, [arXiv:1608.07648 \[astro-ph.CO\]](https://arxiv.org/abs/1608.07648).

[12] **PandaX-II** Collaboration, X. Cui *et al.*, “Dark Matter Results From 54-Ton-Day Exposure of PandaX-II Experiment,” *Phys. Rev. Lett.* **119** no. 18, (2017) 181302, [arXiv:1708.06917 \[astro-ph.CO\]](https://arxiv.org/abs/1708.06917).

[13] **XENON** Collaboration, E. Aprile *et al.*, “Dark Matter Search Results from a One Ton-Year Exposure of XENON1T,” *Phys. Rev. Lett.* **121** no. 11, (2018) 111302, [arXiv:1805.12562 \[astro-ph.CO\]](https://arxiv.org/abs/1805.12562).

[14] **PICO** Collaboration, C. Amole *et al.*, “Dark Matter Search Results from the Complete Exposure of the PICO-60 C_3F_8 Bubble Chamber,” *Phys. Rev. D* **100** no. 2, (2019) 022001, [arXiv:1902.04031 \[astro-ph.CO\]](https://arxiv.org/abs/1902.04031).

[15] T. Daylan, D. P. Finkbeiner, D. Hooper, T. Linden, S. K. N. Portillo, N. L. Rodd, and T. R. Slatyer, “The characterization of the gamma-ray signal from the central Milky Way: A case for annihilating dark matter,” *Phys. Dark Univ.* **12** (2016) 1–23, [arXiv:1402.6703 \[astro-ph.HE\]](https://arxiv.org/abs/1402.6703).

[16] **MAGIC, Fermi-LAT** Collaboration, M. L. Ahnen *et al.*, “Limits to Dark Matter Annihilation Cross-Section from a Combined Analysis of MAGIC and Fermi-LAT Observations of Dwarf Satellite Galaxies,” *JCAP* **02** (2016) 039, [arXiv:1601.06590 \[astro-ph.HE\]](https://arxiv.org/abs/1601.06590).

[17] T. Lin, “Dark matter models and direct detection,” *PoS* **333** (2019) 009, [arXiv:1904.07915 \[hep-ph\]](https://arxiv.org/abs/1904.07915).

[18] L. J. Hall, K. Jedamzik, J. March-Russell, and S. M. West, “Freeze-In Production of FIMP Dark Matter,” *JHEP* **03** (2010) 080, [arXiv:0911.1120 \[hep-ph\]](https://arxiv.org/abs/0911.1120).

[19] N. Bernal, M. Heikinheimo, T. Tenkanen, K. Tuominen, and V. Vaskonen, “The Dawn of FIMP Dark Matter: A Review of Models and Constraints,” *Int. J. Mod. Phys. A* **32** no. 27, (2017) 1730023, [arXiv:1706.07442 \[hep-ph\]](https://arxiv.org/abs/1706.07442).

[20] R. Essig, J. Mardon, and T. Volansky, “Direct Detection of Sub-GeV Dark Matter,” *Phys. Rev. D* **85** (2012) 076007, [arXiv:1108.5383 \[hep-ph\]](https://arxiv.org/abs/1108.5383).

[21] R. Essig, T. Volansky, and T.-T. Yu, “New Constraints and Prospects for sub-GeV Dark Matter Scattering off Electrons in Xenon,” *Phys. Rev. D* **96** no. 4, (2017) 043017, [arXiv:1703.00910 \[hep-ph\]](https://arxiv.org/abs/1703.00910).

[22] T. Emken, C. Kouvaris, and I. M. Shoemaker, “Terrestrial Effects on Dark Matter-Electron Scattering Experiments,” *Phys. Rev. D* **96** no. 1, (2017) 015018, [arXiv:1702.07750 \[hep-ph\]](https://arxiv.org/abs/1702.07750).

[23] D. Green and S. Rajendran, “The Cosmology of Sub-MeV Dark Matter,” *JHEP* **10** (2017) 013, [arXiv:1701.08750 \[hep-ph\]](https://arxiv.org/abs/1701.08750).

[24] R. Essig, M. Fernandez-Serra, J. Mardon, A. Soto, T. Volansky, and T.-T. Yu, “Direct Detection of sub-GeV Dark Matter with Semiconductor Targets,” *JHEP* **05** (2016) 046, [arXiv:1509.01598 \[hep-ph\]](https://arxiv.org/abs/1509.01598).

[25] R. Essig, A. Manalaysay, J. Mardon, P. Sorensen, and T. Volansky, “First Direct Detection Limits on sub-GeV Dark Matter from XENON10,” *Phys. Rev. Lett.* **109** (2012) 021301, [arXiv:1206.2644 \[astro-ph.CO\]](https://arxiv.org/abs/1206.2644).

[26] N. Bernal, X. Chu, and J. Pradler, “Simply split strongly interacting massive particles,” *Phys. Rev. D* **95** no. 11, (2017) 115023, [arXiv:1702.04906 \[hep-ph\]](https://arxiv.org/abs/1702.04906).

[27] P. Q. Hung, “A Model of electroweak-scale right-handed neutrino mass,” *Phys. Lett. B* **649** (2007) 275–279, [arXiv:hep-ph/0612004](https://arxiv.org/abs/hep-ph/0612004).

[28] P. Q. Hung, “Topologically stable, finite-energy electroweak-scale monopoles,” *Nucl. Phys. B* **962** (2021) 115278, [arXiv:2003.02794 \[hep-ph\]](https://arxiv.org/abs/2003.02794).

[29] J. Ellis, P. Q. Hung, and N. E. Mavromatos, “An electroweak monopole, Dirac quantization and the weak mixing angle,” *Nucl. Phys. B* **969** (2021) 115468, [arXiv:2008.00464 \[hep-ph\]](https://arxiv.org/abs/2008.00464).

[30] V. Hoang, P. Q. Hung, and A. S. Kamat, “Non-sterile electroweak-scale right-handed neutrinos and the dual nature of the 125-GeV scalar,” *Nucl. Phys. B* **896** (2015) 611–656, [arXiv:1412.0343 \[hep-ph\]](https://arxiv.org/abs/1412.0343).

[31] M. E. Peskin and T. Takeuchi, “Estimation of oblique electroweak corrections,” *Phys. Rev. D* **46** (1992) 381–409.

[32] V. Hoang, P. Q. Hung, and A. S. Kamat, “Electroweak precision constraints on the electroweak-scale right-handed neutrino model,” *Nucl. Phys. B* **877** (2013) 190–232, [arXiv:1303.0428 \[hep-ph\]](https://arxiv.org/abs/1303.0428).

[33] **Belle** Collaboration, Y. Miyazaki *et al.*, “Search for Lepton Flavor Violating tau Decays into Three Leptons,” *Phys. Lett. B* **660** (2008) 154–160, [arXiv:0711.2189 \[hep-ex\]](https://arxiv.org/abs/0711.2189).

[34] **MEG II** Collaboration, A. M. Baldini *et al.*, “The design of the MEG II experiment,” *Eur. Phys. J. C* **78** no. 5, (2018) 380, [arXiv:1801.04688 \[physics.ins-det\]](https://arxiv.org/abs/1801.04688).

[35] **SINDRUM II** Collaboration, C. Dohmen *et al.*, “Test of lepton flavor conservation in mu → e conversion on titanium,” *Phys. Lett. B* **317** (1993) 631–636.

[36] **MEG** Collaboration, A. M. Baldini *et al.*, “Search for the lepton flavour violating decay $\mu^+ \rightarrow e^+ \gamma$ with the full dataset of the MEG experiment,” *Eur. Phys. J. C* **76** no. 8, (2016) 434, [arXiv:1605.05081 \[hep-ex\]](https://arxiv.org/abs/1605.05081).

[37] P. Hung, T. Le, V. Q. Tran, and T.-C. Yuan, “Muon-to-Electron Conversion in Mirror Fermion Model with Electroweak Scale Non-Sterile Right-handed Neutrinos,” *Nucl. Phys. B* **932** (2018) 471–504, [arXiv:1701.01761 \[hep-ph\]](https://arxiv.org/abs/1701.01761).

[38] P. Q. Hung, T. Le, V. Q. Tran, and T.-C. Yuan, “Lepton Flavor Violating Radiative Decays in EW-Scale ν_R Model: An Update,” *JHEP* **12** (2015) 169, [arXiv:1508.07016 \[hep-ph\]](https://arxiv.org/abs/1508.07016).

[39] P. Q. Hung, “Electroweak-scale mirror fermions, mu → e gamma and tau → mu gamma,” *Phys. Lett. B* **659** (2008) 585–592, [arXiv:0711.0733 \[hep-ph\]](https://arxiv.org/abs/0711.0733).

[40] P. Hung, “A non-vanishing neutrino mass and the strong CP problem: A new solution from the perspective of the EW- ν_R model,” in *Meeting of the APS Division of Particles and Fields*. 2017. [arXiv:1710.00498 \[hep-ph\]](https://arxiv.org/abs/1710.00498).

[41] P. Q. Hung, “Mirror fermions and the strong CP problem: A new axionless solution and experimental implications,” [arXiv:1712.09701 \[hep-ph\]](https://arxiv.org/abs/1712.09701).

[42] **CMS** Collaboration, A. M. Sirunyan *et al.*, “Combined measurements of Higgs boson couplings in proton–proton collisions at $\sqrt{s} = 13$ TeV,” *Eur. Phys. J. C* **79** no. 5, (2019) 421, [arXiv:1809.10733 \[hep-ex\]](https://arxiv.org/abs/1809.10733).

[43] **CMS** Collaboration, S. Chatrchyan *et al.*, “Observation of a new boson at a mass of 125 GeV with

the CMS experiment at the LHC,” *Phys. Lett.* **B716** (2012) 30–61, [arXiv:1207.7235 \[hep-ex\]](https://arxiv.org/abs/1207.7235).

[44] **ATLAS** Collaboration, G. Aad *et al.*, “Observation of a new particle in the search for the Standard Model Higgs boson with the ATLAS detector at the LHC,” *Phys. Lett.* **B716** (2012) 1–29, [arXiv:1207.7214 \[hep-ex\]](https://arxiv.org/abs/1207.7214).

[45] T. D. Lee, “A Theory of Spontaneous T Violation,” *Phys. Rev. D* **8** (1973) 1226–1239.

[46] A. Wahab El Kaffas, P. Osland, and O. M. Ogreid, “Constraining the Two-Higgs-Doublet-Model parameter space,” *Phys. Rev. D* **76** (2007) 095001, [arXiv:0706.2997 \[hep-ph\]](https://arxiv.org/abs/0706.2997).

[47] G. C. Branco, P. M. Ferreira, L. Lavoura, M. N. Rebelo, M. Sher, and J. P. Silva, “Theory and phenomenology of two-Higgs-doublet models,” *Phys. Rept.* **516** (2012) 1–102, [arXiv:1106.0034 \[hep-ph\]](https://arxiv.org/abs/1106.0034).

[48] S. Chakdar, K. Ghosh, V. Hoang, P. Q. Hung, and S. Nandi, “The search for electroweak-scale right-handed neutrinos and mirror charged leptons through like-sign dilepton signals,” *Phys. Rev. D* **95** no. 1, (2017) 015014, [arXiv:1606.08502 \[hep-ph\]](https://arxiv.org/abs/1606.08502).

[49] C. Rott, K. Kohri, and S. C. Park, “Superheavy dark matter and IceCube neutrino signals: Bounds on decaying dark matter,” *Phys. Rev. D* **92** no. 2, (2015) 023529, [arXiv:1408.4575 \[hep-ph\]](https://arxiv.org/abs/1408.4575).

[50] M. Re Fiorentin, V. Niro, and N. Fornengo, “A consistent model for leptogenesis, dark matter and the IceCube signal,” *JHEP* **11** (2016) 022, [arXiv:1606.04445 \[hep-ph\]](https://arxiv.org/abs/1606.04445).

[51] B. Audren, J. Lesgourgues, G. Mangano, P. D. Serpico, and T. Tram, “Strongest model-independent bound on the lifetime of Dark Matter,” *JCAP* **12** (2014) 028, [arXiv:1407.2418 \[astro-ph.CO\]](https://arxiv.org/abs/1407.2418).

[52] **IceCube** Collaboration, M. Aartsen *et al.*, “Observation of High-Energy Astrophysical Neutrinos in Three Years of IceCube Data,” *Phys. Rev. Lett.* **113** (2014) 101101, [arXiv:1405.5303 \[astro-ph.HE\]](https://arxiv.org/abs/1405.5303).

[53] E. W. Kolb and M. S. Turner, *The early universe*. Frontiers in physics. Westview Press, Boulder, CO, 1990. <https://cds.cern.ch/record/206230>.

[54] M. Bauer and T. Plehn, *Yet Another Introduction to Dark Matter: The Particle Physics Approach*, vol. 959 of *Lecture Notes in Physics*. Springer, 2019. [arXiv:1705.01987 \[hep-ph\]](https://arxiv.org/abs/1705.01987).

[55] A. Biswas and A. Gupta, “Freeze-in Production of Sterile Neutrino Dark Matter in $U(1)_{B-L}$ Model,” *JCAP* **09** (2016) 044, [arXiv:1607.01469 \[hep-ph\]](https://arxiv.org/abs/1607.01469). [Addendum: *JCAP* 05, A01 (2017)].

[56] P. Gondolo and G. Gelmini, “Cosmic abundances of stable particles: Improved analysis,” *Nucl.*

Phys. B **360** (1991) 145–179.

[57] **Particle Data Group** Collaboration, P. Zyla *et al.*, “Review of Particle Physics,” PTEP **2020** no. 8, (2020) 083C01.

[58] A. Djouadi, J. Kalinowski, and P. Zerwas, “Two and three-body decay modes of SUSY Higgs particles,” Z. Phys. C **70** (1996) 435–448, [arXiv:hep-ph/9511342](https://arxiv.org/abs/hep-ph/9511342).

[59] D. Borah, B. Karmakar, and D. Nanda, “Common Origin of Dirac Neutrino Mass and Freeze-in Massive Particle Dark Matter,” JCAP **07** (2018) 039, [arXiv:1805.11115](https://arxiv.org/abs/1805.11115) [hep-ph].

[60] S. Peyman Zakeri, S. Mohammad Moosavi Nejad, M. Zakeri, and S. Yaser Ayazi, “A Minimal Model For Two-Component FIMP Dark Matter: A Basic Search,” Chin. Phys. C **42** no. 7, (2018) 073101, [arXiv:1801.09115](https://arxiv.org/abs/1801.09115) [hep-ph].

[61] J. Herms and A. Ibarra, “Probing multicomponent FIMP scenarios with gamma-ray telescopes,” JCAP **03** (2020) 026, [arXiv:1912.09458](https://arxiv.org/abs/1912.09458) [hep-ph].

[62] F. D’Eramo and A. Lenoci, “Lower Mass Bounds on FIMPs,” [arXiv:2012.01446](https://arxiv.org/abs/2012.01446) [hep-ph].

[63] P. Das, M. K. Das, and N. Khan, “The FIMP-WIMP dark matter and Muon g-2 in the extended singlet scalar model,” [arXiv:2104.03271](https://arxiv.org/abs/2104.03271) [hep-ph].

[64] P. Das, M. K. Das, and N. Khan, “Extension of Hyperchargeless Higgs Triplet Model,” [arXiv:2107.01578](https://arxiv.org/abs/2107.01578) [hep-ph].

[65] M. Pandey, D. Majumdar, and K. P. Modak, “Two Component Feebly Interacting Massive Particle (FIMP) Dark Matter,” JCAP **06** (2018) 023, [arXiv:1709.05955](https://arxiv.org/abs/1709.05955) [hep-ph].

[66] A. Biswas, S. Choubey, and S. Khan, “Neutrino mass, leptogenesis and FIMP dark matter in a $U(1)_{B-L}$ model,” Eur. Phys. J. C **77** no. 12, (2017) 875, [arXiv:1704.00819](https://arxiv.org/abs/1704.00819) [hep-ph].

[67] C. E. Yaguna, “The Singlet Scalar as FIMP Dark Matter,” JHEP **08** (2011) 060, [arXiv:1105.1654](https://arxiv.org/abs/1105.1654) [hep-ph].

[68] D. Borah, D. Nanda, and A. K. Saha, “Common origin of modified chaotic inflation, nonthermal dark matter, and Dirac neutrino mass,” Phys. Rev. D **101** no. 7, (2020) 075006, [arXiv:1904.04840](https://arxiv.org/abs/1904.04840) [hep-ph].

[69] D. Gruber, J. Matteson, L. Peterson, and G. Jung, “The spectrum of diffuse cosmic hard x-rays measured with heao-1,” Astrophys. J. **520** (1999) 124, [arXiv:astro-ph/9903492](https://arxiv.org/abs/astro-ph/9903492).

[70] L. Bouchet, E. Jourdain, J. Roques, A. Strong, R. Diehl, F. Lebrun, and R. Terrier, “INTEGRAL

SPI All-Sky View in Soft Gamma Rays: Study of Point Source and Galactic Diffuse Emissions,” *Astrophys. J.* **679** (2008) 1315, [arXiv:0801.2086 \[astro-ph\]](https://arxiv.org/abs/0801.2086).

[71] P. S. Bhupal Dev, A. Mazumdar, and S. Qutub, “Constraining Non-thermal and Thermal properties of Dark Matter,” *Front. in Phys.* **2** (2014) 26, [arXiv:1311.5297 \[hep-ph\]](https://arxiv.org/abs/1311.5297).

[72] G. Choi, T. T. Yanagida, and N. Yokozaki, “Feebly interacting $U(1)_{B-L}$ gauge boson warm dark matter and XENON1T anomaly,” *Phys. Lett. B* **810** (2020) 135836, [arXiv:2007.04278 \[hep-ph\]](https://arxiv.org/abs/2007.04278).

[73] R. Essig, E. Kuflik, S. D. McDermott, T. Volansky, and K. M. Zurek, “Constraining Light Dark Matter with Diffuse X-Ray and Gamma-Ray Observations,” *JHEP* **11** (2013) 193, [arXiv:1309.4091 \[hep-ph\]](https://arxiv.org/abs/1309.4091).

[74] **Fermi-LAT** Collaboration, M. Ackermann *et al.*, “Fermi LAT Search for Dark Matter in Gamma-ray Lines and the Inclusive Photon Spectrum,” *Phys. Rev. D* **86** (2012) 022002, [arXiv:1205.2739 \[astro-ph.HE\]](https://arxiv.org/abs/1205.2739).

[75] M. Cirelli, P. Panci, and P. D. Serpico, “Diffuse gamma ray constraints on annihilating or decaying Dark Matter after Fermi,” *Nucl. Phys. B* **840** (2010) 284–303, [arXiv:0912.0663 \[astro-ph.CO\]](https://arxiv.org/abs/0912.0663).

[76] K. S. C., *Ph. D. Thesis*. PhD thesis, University of New Hampshire, USA, 1998.

[77] A. W. Strong, I. V. Moskalenko, and O. Reimer, “Diffuse galactic continuum gamma rays. A Model compatible with EGRET data and cosmic-ray measurements,” *Astrophys. J.* **613** (2004) 962–976, [arXiv:astro-ph/0406254](https://arxiv.org/abs/astro-ph/0406254).

[78] **XENON100** Collaboration, E. Aprile *et al.*, “Dark Matter Results from 100 Live Days of XENON100 Data,” *Phys. Rev. Lett.* **107** (2011) 131302, [arXiv:1104.2549 \[astro-ph.CO\]](https://arxiv.org/abs/1104.2549).

[79] **XENON100** Collaboration, E. Aprile *et al.*, “Dark Matter Results from 225 Live Days of XENON100 Data,” *Phys. Rev. Lett.* **109** (2012) 181301, [arXiv:1207.5988 \[astro-ph.CO\]](https://arxiv.org/abs/1207.5988).

[80] **LUX** Collaboration, D. S. Akerib *et al.*, “First results from the LUX dark matter experiment at the Sanford Underground Research Facility,” *Phys. Rev. Lett.* **112** (2014) 091303, [arXiv:1310.8214 \[astro-ph.CO\]](https://arxiv.org/abs/1310.8214).

[81] D. M. Mei, G. J. Wang, H. Mei, G. Yang, J. Liu, M. Wagner, R. Panth, K. Kooi, Y. Y. Yang, and W. Z. Wei, “Direct Detection of MeV-Scale Dark Matter Utilizing Germanium Internal Amplification for the Charge Created by the Ionization of Impurities,” *Eur. Phys. J. C* **78** no. 3, (2018) 187, [arXiv:1708.06594 \[physics.ins-det\]](https://arxiv.org/abs/1708.06594).

- [82] T. Trickle, Z. Zhang, and K. M. Zurek, “Detecting Light Dark Matter with Magnons,” *Phys. Rev. Lett.* **124** no. 20, (2020) 201801, [arXiv:1905.13744 \[hep-ph\]](https://arxiv.org/abs/1905.13744).
- [83] J. M. No, P. Tunney, and B. Zaldivar, “Probing Dark Matter freeze-in with long-lived particle signatures: MATHUSLA, HL-LHC and FCC-hh,” *JHEP* **03** (2020) 022, [arXiv:1908.11387 \[hep-ph\]](https://arxiv.org/abs/1908.11387).
- [84] S. Chakdar, K. Ghosh, V. Hoang, P. Q. Hung, and S. Nandi, “Search for mirror quarks at the LHC,” *Phys. Rev. D* **93** no. 3, (2016) 035007, [arXiv:1508.07318 \[hep-ph\]](https://arxiv.org/abs/1508.07318).
- [85] S. Chakdar and P. Q. Hung, “Prospect of the Electroweak Scale Right-handed neutrino model in the Lifetime Frontier,” in *International Conference on Neutrinos and Dark Matter*. 5, 2020. [arXiv:2006.00381 \[hep-ph\]](https://arxiv.org/abs/2006.00381).
- [86] K. Hartling, K. Kumar, and H. E. Logan, “The decoupling limit in the Georgi-Machacek model,” *Phys. Rev. D* **90** no. 1, (2014) 015007, [arXiv:1404.2640 \[hep-ph\]](https://arxiv.org/abs/1404.2640).